



# Cosmogenic $^{10}\text{Be}$ constraints on Little Ice Age glacial advances in the eastern Tian Shan, China



Yanan Li <sup>a</sup>, Yingkui Li <sup>b,\*</sup>, Jon Harbor <sup>c</sup>, Gengnian Liu <sup>d</sup>, Chaolu Yi <sup>e</sup>, Marc W. Caffee <sup>c,f</sup>

<sup>a</sup> Department of Geography, South Dakota State University, Brookings, SD 57007, USA

<sup>b</sup> Department of Geography, The University of Tennessee, Knoxville, TN 37996, USA

<sup>c</sup> Department of Earth, Atmospheric, and Planetary Sciences, Purdue University, West Lafayette, IN 47907, USA

<sup>d</sup> College of Urban and Environmental Sciences, Peking University, Beijing 100871, China

<sup>e</sup> Institute of Tibetan Plateau Research, Chinese Academy of Sciences, CAS Center for Excellence in Tibetan Plateau Earth Sciences, Beijing 100085, China

<sup>f</sup> Department of Physics and Astronomy, Purdue University, West Lafayette, IN 47907, USA

## ARTICLE INFO

### Article history:

Received 10 September 2015

Received in revised form

3 January 2016

Accepted 19 February 2016

Available online 12 March 2016

### Keywords:

Cosmogenic nuclides

Little Ice Age glacial advances

Nuclide inheritance

Eastern Tian Shan

## ABSTRACT

Presumed Little Ice Age (LIA) glacial advances, represented by a set of fresh, sharp-crested, boulder covered and compact moraines a few hundred meters downstream from modern glaciers, have been widely recognized in the Central Asian highlands. However, few studies have constrained the formation ages of these moraines. We report 31  $^{10}\text{Be}$  exposure ages from presumed LIA moraines in six glacial valleys in the Urumqi River headwater area and the Haxilegen Pass area of the eastern Tian Shan, China. Our results reveal that the maximum LIA glacial extent occurred mainly around  $430 \pm 100$  yr, a cold and wet period as indicated by proxy data from ice cores, tree rings, and lake sediments in Central Asia. We also dated a later glacial advance to  $270 \pm 55$  yr. However,  $^{10}\text{Be}$  exposure ages on several presumed LIA moraines in front of small, thin glaciers are widely scattered and much older than the globally recognized timing of the LIA. Historical topographic maps indicate that most glaciers were more extensive in the early 1960s, and two of our  $^{10}\text{Be}$  sample sites were located close to the ice front at that time. Boulders transported by these small and thin glaciers may be reworked from deposits originally formed prior to the LIA glacial advances, producing apparently old and widely scattered exposure ages due to varied nuclide inheritance. Other published ages indicated an earlier LIA advance around  $790 \pm 300$  yr in the easternmost Tian Shan, but in our study area the more extensive advance around  $430 \pm 100$  yr likely reworked or covered deposits from this earlier event.

© 2016 Elsevier Ltd. All rights reserved.

## 1. Introduction

The “Little Ice Age” (LIA) is a well-recognized cold period in the past millennium that occurred between approximately 1300 CE and 1850 CE (Grove, 2004; Mann et al., 2009). The timing and intensity of this cold event have been documented in historical records and natural proxies around the world, including tree rings, sediments, and ice cores (e.g. Yao et al., 1997; Luckman, 2000; Grove, 2004; Solomina et al., 2004; Harrison et al., 2007; Mann et al., 2008, 2009; Chenet et al., 2010; Chen et al., 2013; Xu and Yi, 2014). Abundant evidence show that, in many parts of the world, glaciers were more extensive during the period of 1300–1850 CE than they were at the beginning of the last

millennium and since the twentieth century (e.g. Benedict, 1968; Mosley-Thompson et al., 1990; Koch and Kilian, 2005; Bräuning, 2006; Barclay et al., 2009; Schaefer et al., 2009; Xu and Yi, 2014). The timing and extent of LIA glacial advances are highly variable around the world, and LIA cooling was probably not a globally synchronous event (Bradley and Jones, 1993; Kreutz et al., 1997; Mann et al., 1999; Mann, 2002; Chenet et al., 2010; Luthi, 2014).

In introducing the term “Little Ice Age”, Matthes (1939) observed that “... many of the small cirque glaciers on those ranges (mountain ranges in the western U.S.) are fronted by very fresh-looking terminal moraines arranged in compact concentric series or combined into one or two massive compound embankments ...” (page 520). Glacial landforms with similar characteristics also exist in the Tibetan Plateau and its surrounding mountains (e.g. Shi and Ren, 1990; Su and Shi, 2002; Owen, 2009; Li et al., 2014; Xu and Yi, 2014; Chen et al., 2015). Some of these

\* Corresponding author.

E-mail address: [yli32@utk.edu](mailto:yli32@utk.edu) (Y. Li).

moraines have been dated using radiocarbon, dendrochronology, and lichenometry based on proxy materials, such as buried wood, trees, and lichens (e.g. Derbyshire et al., 1984; Luckman, 2000; Solomina et al., 2004; Jiao et al., 2005; Bräuning, 2006; Loso et al., 2014). It is challenging to accurately constrain the timing of LIA glacial advances in many locations, including the Central Asian highlands, because of the lack of proxy materials for these methods. Cosmogenic nuclide (mainly  $^{10}\text{Be}$ ) surface exposure dating has been widely used to constrain the timing of Quaternary glacial events (Gosse and Phillips, 2001; Ivy-Ochs and Kober, 2008; Li and Harbor, 2009). One advantage of this method is that the material needed for dating (boulders or sediments) is ubiquitous in glacial environments. The time range for cosmogenic nuclide surface exposure dating spans from hundreds to millions of years. In the past decade, several studies have successfully used this method to date young glacial deposits on the  $10^2$  year time-scale (e.g. Finkel et al., 2003; Owen et al., 2005; Kelly et al., 2008; Koppes et al., 2008; Schaefer et al., 2009; Seong et al., 2009; Li et al., 2014; Winsor et al., 2014; Chen et al., 2015). These studies demonstrated the potential of using cosmogenic nuclide surface exposure dating to constrain the age of LIA deposits.

Constraining the timing and extent of past glacial events is of critical importance for understanding past climate conditions and assessing future glacial and environmental changes. Located at the confluence zone of the westerlies and the Siberian High, mountain glaciers in the Tian Shan are sensitive indicators of climate change (Benn and Owen, 1998; Aizen et al., 2001; Sorg et al., 2012). Glaciers are particularly important today because they provide freshwater supply for natural and human ecosystems in the arid and semi-arid area of Central Asia. Ongoing glacial retreat is a rising concern for the water availability and food security in this rapidly developing region. Previous paleo-glacial reconstructions have been conducted to establish glacial chronologies in the Tian Shan (e.g. Zhao et al., 2006; Narama et al., 2007; Koppes et al., 2008; Kong et al., 2009; Li et al., 2011, 2014; Zech, 2012; Lifton et al., 2014; Chen et al., 2015). Only a few studies have constrained the formation ages of LIA moraines, using cosmogenic  $^{10}\text{Be}$  exposure dating (Koppes et al., 2008; Li et al., 2014; Chen et al., 2015), lichenometry (Chen, 1989; Solomina et al., 2004), or radiocarbon dating (Yi et al., 2004).

The purpose of this study is to constrain the formation ages of presumed LIA moraines from six glacial valleys in the Urumqi River source area and the Haxilegen Pass area of the eastern Tian Shan, China, using cosmogenic  $^{10}\text{Be}$  surface exposure dating. Combined with other published LIA ages, we then examine the timing and pattern of LIA glacial advances across the eastern Tian Shan. We also compare our glacial chronology with proxy climate records derived from tree rings, sediment cores, ice cores, and other materials to examine the relationship between glacier changes and climate fluctuations during the LIA.

## 2. Study area

The Tian Shan is one of the largest mountain ranges in Central Asia, formed by collision of the Indian and Eurasian continental plates about 40–50 million years ago (Yin and Harrison, 2000; Kaban and Yuanda, 2014). It includes a series of WSW–ENE trending ranges, stretching from the western boundary of Kyrgyzstan across the Xinjiang Uighur Autonomous Region in China and almost to Mongolia (Fig. 1). Many high peaks in these ranges reach over 4000 m above sea level (a.s.l.). The Tian Shan is bounded by the Taklamakan Desert to the south and the Gurbantonggut Desert to the north, producing a distinct contrast of environments between high mountains and intervening valleys/basins (Aizen et al., 1997). The continental climate of this area has high aridity and extremes of seasonal and diurnal temperatures (Aizen et al., 1997; Ye et al.,

2005). The prevalent westerlies bring moisture from the Aral, Caspian, and Black Seas, as well as from the North Atlantic and Arctic Oceans, and they interact with the mountain ranges, causing a sharp west–east decreasing gradient in precipitation (orographic effect) (Benn and Owen, 1998; Aizen et al., 2006; Chen et al., 2008; Sorg et al., 2012). The Siberian High is another important climate system in this area, and is mainly associated with cold and dry winters (Gong and Ho, 2002; Yang et al., 2009). Asian monsoon systems do not typically penetrate into the Tian Shan due to the orographic barriers formed by the Himalayas and the Tibetan Plateau (Fig. 1; Chen et al., 2008). Large valley glaciers and ice caps occur mainly in the western Tian Shan where high elevations induce cold environment and receive more moisture from the westerlies, while the eastern Tian Shan (Chinese Tian Shan) contains relatively small glaciers due to relatively lower elevations and limited precipitation.

We investigated two areas in the eastern Tian Shan: the headwaters of the Urumqi River and the Haxilegen Pass (Figs. 2 and 3). These two areas are located west of Urumqi, the capital city of the Xinjiang Uyghur Autonomous Regions, China, and are about 200 km apart. The headwater area of the Urumqi River ( $\sim 43.10^\circ\text{N}$ ,  $86.83^\circ\text{E}$ ) is located in the Tianger Range with a mean annual temperature of about  $-5.6^\circ\text{C}$  and an annual precipitation of about 430 mm (Liu and Xiong, 1992). The Haxilegen Pass ( $\sim 43.73^\circ\text{N}$ ,  $84.41^\circ\text{E}$ ) is located in the Borohoro Range. The mean annual temperature is about  $-5.2^\circ\text{C}$  on the southern slope, and  $-5.8^\circ\text{C}$  on the northern slope of the pass, and the annual precipitation is about 500–600 mm (Liu and Xiong, 1992). Modern glaciers in both areas are characterized with small valley glaciers, hanging glaciers, and cirque glaciers that are mainly preserved on the northern slopes of the mountain range, whereas abundant geomorphic evidence, such as erratics, striations, moraines, and U-shaped valleys, are preserved around high peak areas, indicating that these areas have been glaciated in the past (Cui, 1981; Liu and Xiong, 1992; Li et al., 2001a, 2001b). Our field investigation focused on the presumed LIA moraines in front of six modern glaciers (three glaciers in each area).

## 3. Geomorphologic setting and previous work

### 3.1. Headwaters of the Urumqi River

The Urumqi River headwater area is well known in the field of glacial geomorphology due to its accessibility, well-preserved glacial landforms, and the presence of the Tian Shan Glaciological Station, established by the Chinese Academy of Sciences in 1959. Our samples were collected in front of three glaciers: Glacier No. 1 (UG1), Glacier No. 3 (UG3), and a glacier on the southern slope of the ridge (UGS) (Fig. 2a).

UG1 and UG3 are located in the head of the Daxi Valley, an east-facing U-shaped valley with double troughs on the northern slope of the mountain range (Cui, 1981; Li et al., 2001a). Meltwater from UG1, UG3, and other glaciers in this area flows into the Urumqi River and provides freshwater supply for Urumqi City. UG1 is one of the most intensively studied glaciers in Central Asia. It currently has two branches that were part of a single larger glacier in the early 1990s (Li et al., 2008), and it was much larger in the early 1960s as illustrated on the historic topographic maps (Fig. 2a; Li et al., 2001a). The total area of the current two branches is about  $1.6\text{ km}^2$ . The lower branch of UG1 ends at an elevation of 3750 m a.s.l. Compared to UG1, UG3 is a small (area =  $0.4\text{ km}^2$ ) and thin glacier, and it resides on a sheltered steep slope, facing north (Fig. 2a). The glacier front ends at 3660 m a.s.l.

Previous studies have identified several groups of moraines in the Daxi Valley, and a detailed glacial geomorphological map of the

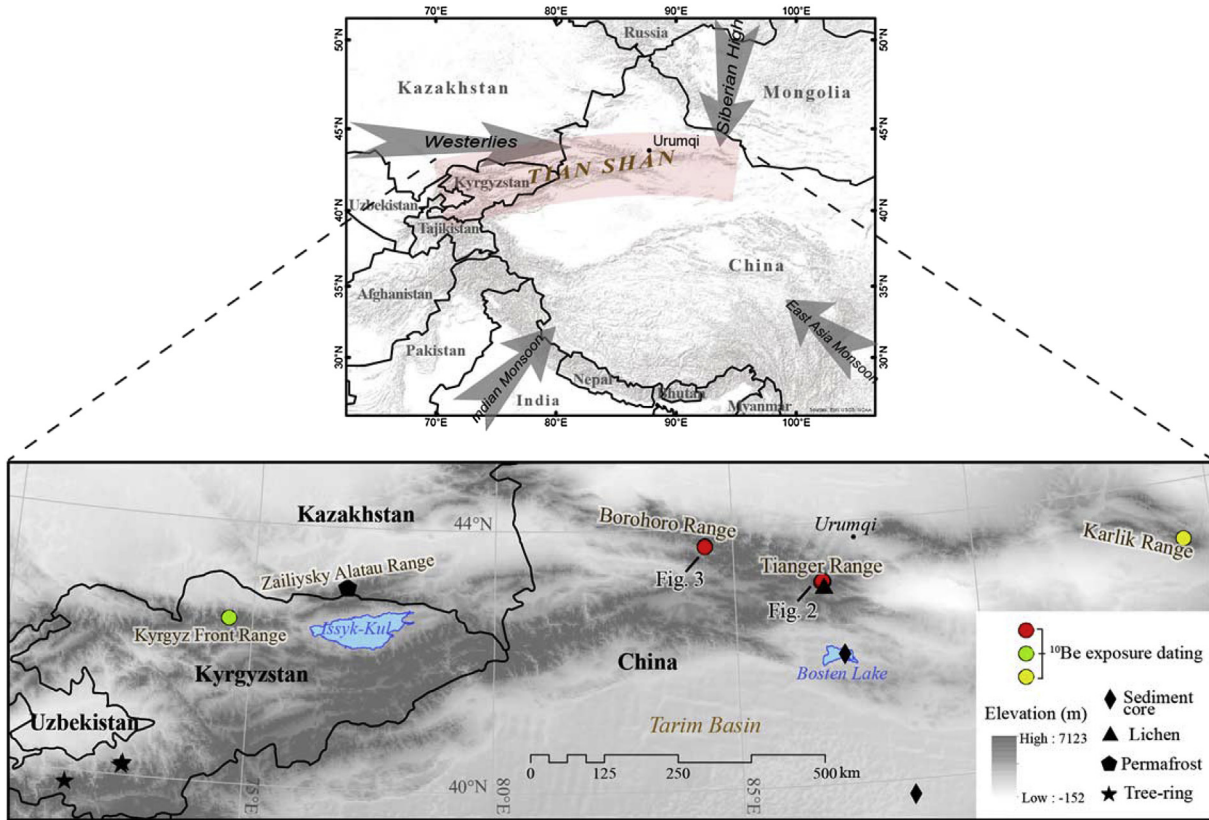


**Fig. 1.** Study area. Upper: Overview map showing the location of the study area (red box) and surrounding atmospheric circulations (grey arrows); Bottom: location of data sites discussed in this paper. Red dots are our  $^{10}\text{Be}$  dating sites; green dots are  $^{10}\text{Be}$  exposure ages in the Kyrgyz Front Range (Koppes et al., 2008); yellow dots are  $^{10}\text{Be}$  exposure ages in the Karlik Range (Chen et al., 2015). Other proxy data sites shown are: a lake sediment core from Bosten lake (Chen et al., 2006); an aeolian sediment section in the Tarim Basin (Liu et al., 2011); lichenometry dating at Glacier No. 1 (Chen, 1989); permafrost layers in the Zailiysky Alatau Range (Marchenko and Gorbunov, 1997); and dendrochronological studies in the western Kyrgyz Tian Shan (Esper et al., 2003). (For interpretation of the references to colour in this figure legend, the reader is referred to the web version of this article.)

Daxi Valley can be found in Li et al. (2011). A set of fresh-looking lateral-terminal moraines are located 700 m downstream from the UG1 lower branch terminus and 400 m downstream from UG3 terminus with limited weathering, soil development, and vegetation cover (Fig. 4a–d). Such fresh moraines are believed to have formed during the LIA (Yang and Qiu, 1965; Zheng, 1990; Wang, 1993). Multiple dating techniques have been used to constrain the formation age of such moraines in front of UG1. Specifically, Chen (1989) dated three moraine ridges to 1595–1650 CE, 1765–1795 CE, and 1820–1900 CE, using lichenometry. Yi et al. (2004) obtained ages of  $1550 \text{ CE} \pm 120$  and  $1520 \pm 120$  (recalculated in Xu and Yi, 2014) using AMS  $^{14}\text{C}$  dating of organic calcium oxalate coatings left by dead lichen on clasts within the moraines. Recently, Li et al. (2014) published ages of four boulders from the outermost terminal moraine around  $400 \pm 70$  yr based on  $^{10}\text{Be}$  exposure dating. The similar fresh-looking moraines in front of UG3 have gentle surfaces (Fig. 4c, d), rather than crested ridges. The formation age of this moraine set has not been constrained previously. Considering the shape, size, and topographic conditions, these moraines might have moved slowly downward as a rock glacier after ice retreat (Liu et al., 1995). Between the fresh-looking moraines of UG1 and the Tian Shan Glaciological Station, a set of moraines, located 1–2 km from UG1 lower terminus, contains slightly weathered boulders and has vegetation grown on the surface. Previous dating results at this site showed a possible formation during the Neoglacial (Zheng and Zhang, 1983), but  $^{10}\text{Be}$  exposure ages, ranging from  $11.5 \pm 0.9$  kyr to  $24.3 \pm 1.8$  kyr from moraine boulders (Fig. 2a; Kong et al., 2009; Li et al., 2011) and an

AMS  $^{14}\text{C}$  age of  $\sim 19$  kyr from the till matrix near the station (Yi et al., 2004) suggested that this moraine set was likely formed during Marine Oxygen Isotope Stage (MIS) 2. Two sets of moraines (Lower Wangfeng and Upper Wangfeng moraines) were preserved further down ( $>10$  km) the Daxi Valley (Cui, 1981; Wang, 1981). Cosmogenic  $^{10}\text{Be}$  exposure ages suggested that these moraines were also formed during MIS 2 (Kong et al., 2009; Li et al., 2011). However, controversy exists due to the disparity in ages from the same moraine constrained using different dating methods. In particular, ages constrained using electron spin resonance (ESR) dating (Yi et al., 2002; Zhao et al., 2006) are much older than the  $^{10}\text{Be}$  exposure ages. This disparity has been explained as caused by the potential incomplete resetting of ESR signals, or the potential impact of moraine degradation on  $^{10}\text{Be}$  surface exposure dating (Li et al., 2011). In a nearby valley (Ala Valley) on the southern slope of the Tianger Range, older glacial stages, such as MIS 3, MIS 4, and MIS 6 or older, were constrained based on  $^{10}\text{Be}$  exposure dating (Li et al., 2014).

The south-facing UGS is a small glacier (area =  $0.2 \text{ km}^2$ ), with a terminal elevation of 4000 m a.s.l. No sharp-crested fresh moraines are distributed within several hundred meters beyond the glacier front. Instead, we only observed some trace-lines in the field that may represent the presumed LIA extent of this glacier (Fig. 4e). The lack of prominent moraine topography in front of UGS suggests that UGS is likely cold-based with limited power to produce enough materials to form distinct moraines in the past. No prior dating work has been conducted at this site.

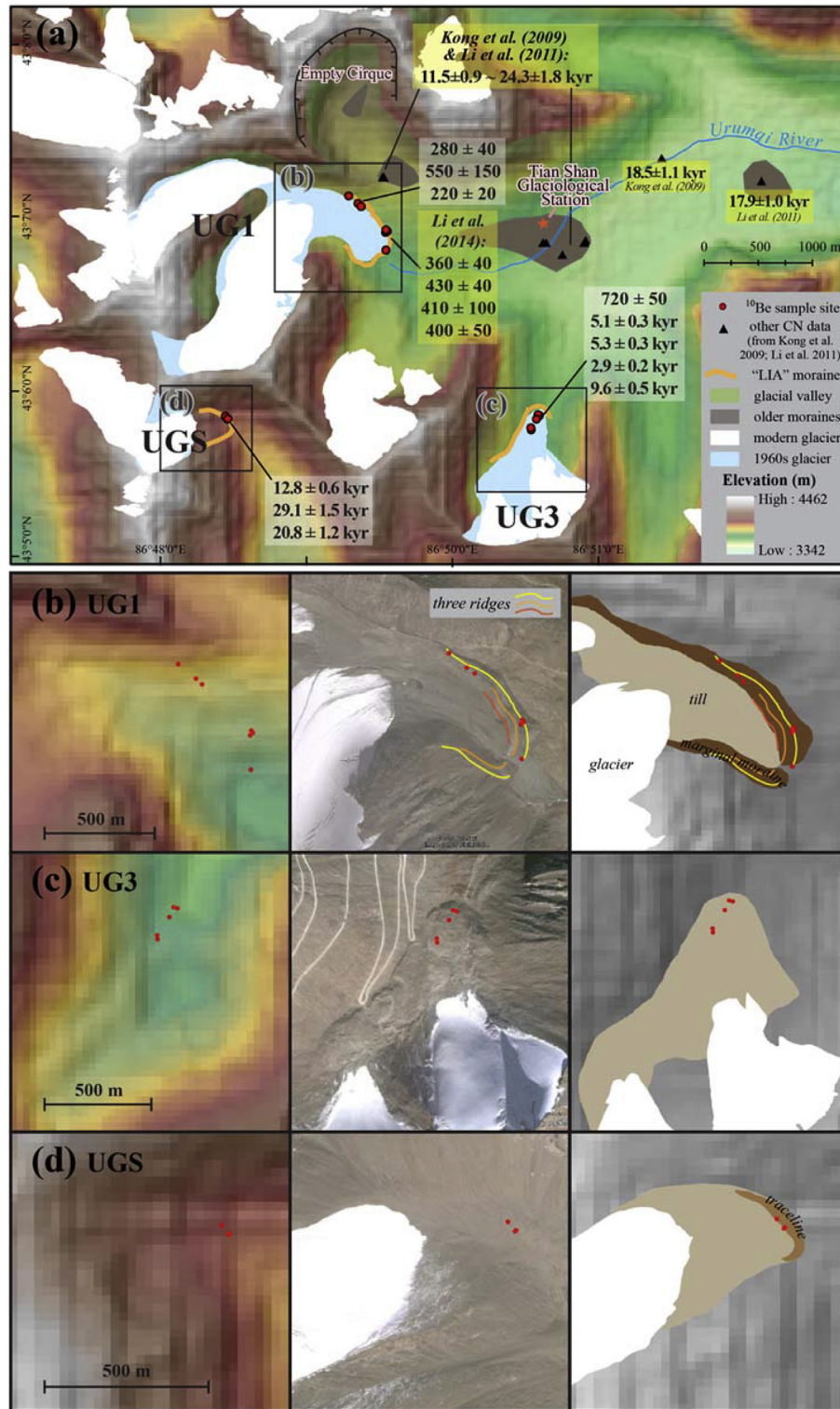


**Fig. 2.** Geomorphologic setting of the Urumqi River headwater area: (a) overview of the sample sites. Modern glaciers are in white, and the 1960s glaciers, derived from historic topographic maps, are in light blue.  $^{10}\text{Be}$  exposure ages (in unit of yr if not labeled) from this study are shown in white boxes, and data from Li et al. (2014) are shown in the yellow box. (b), (c), and (d) are enlarged areas for each sampled glaciers. Three panels in (b), (c), and (d) show the sample sites in hillshaded DEM, in Google Earth, and in illustration of glacial landforms, respectively. (For interpretation of the references to colour in this figure legend, the reader is referred to the web version of this article.)

### 3.2. Haxilegen Pass

In the Haxilegen Pass area, we investigated the LIA moraines in front of three glaciers, named as HDBA, HDBB, and HDBC (Fig. 3).

HDBA and HDBB are located on the northern slope of the ridge, while HDBC is located on the southern slope. The areas of HDBA and HDBB are 1.1 km<sup>2</sup> and 1.2 km<sup>2</sup>, similar to the size of UG1. The right margin of the HDBA fresh moraine merges with the HDBB

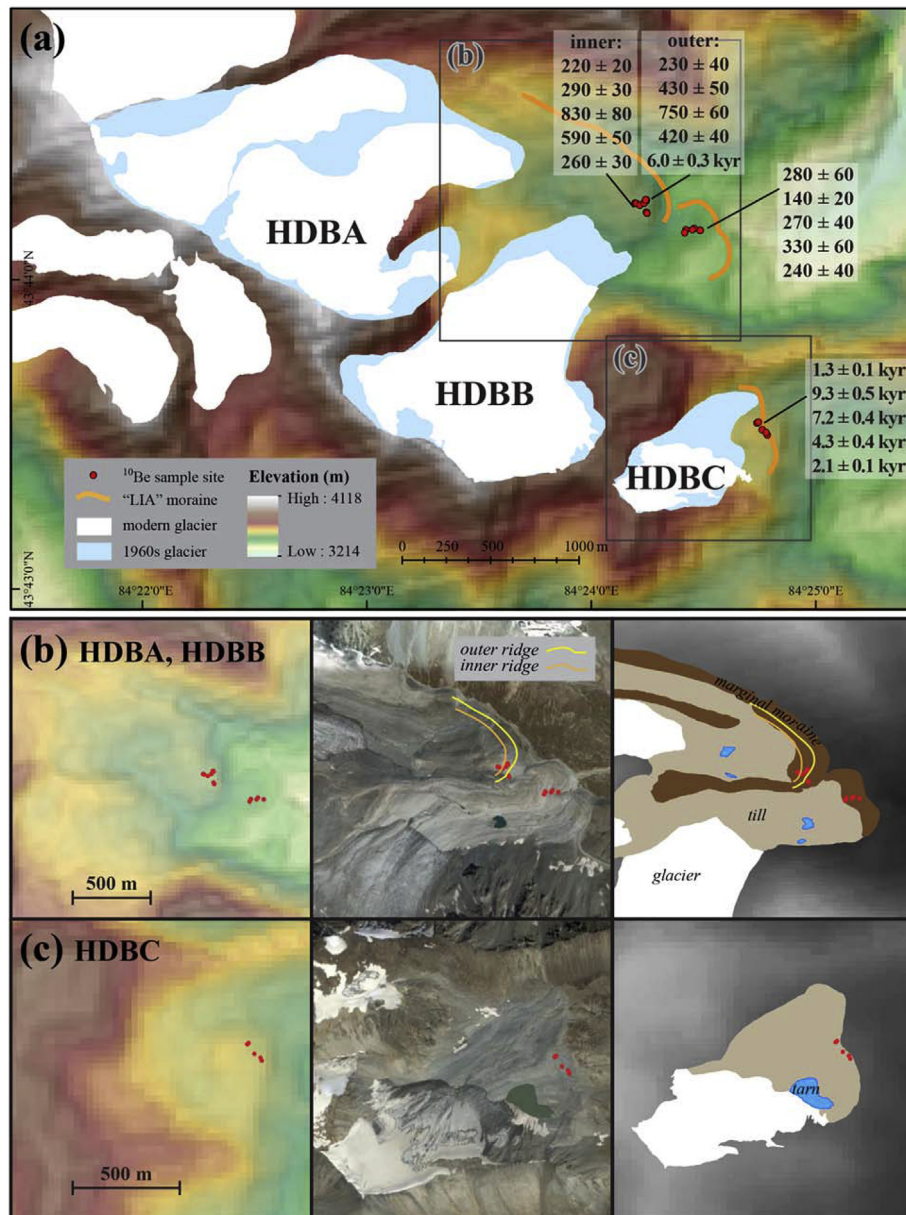


**Fig. 3.** Geomorphic setting of the Haxilegen Pass area: (a) overview of the sample sites. Modern glaciers are in white, and the 1960s glaciers, derived from historic topographic maps, are in light blue.  $^{10}\text{Be}$  exposure ages (in unit of yr if not labeled) from this study are shown in white boxes. (b) and (c) are enlarged areas for sampled glaciers. Three panels in (b) and (c) show the sample sites in hillshaded DEM, in Google Earth, and in illustration of glacial landforms, respectively. (For interpretation of the references to colour in this figure legend, the reader is referred to the web version of this article.)

fresh moraine, but these moraines are still distinguishable in Google Earth imagery and in the field (Figs. 3b and 4f). The fresh moraine of HDBA ends at a higher elevation (3400 m a.s.l.) than that of HDBB (3380 m a.s.l.). Both moraines are rich in boulders, and the height of the fresh, outermost moraine was estimated to be about 10–15 m in the field. The fresh-looking moraines without vegetation cover overlap grass-covered older landforms (Fig. 4f, i). The distance from the fresh moraine to the glacier front is about 900 m. Four small tarns lie between the moraines and the glacier front (Fig. 3b). Large boulders (>1 m in diameter) are scattered on the moraine surfaces (Fig. 4g, h, j). The topographic and geometric setting of HDBC is similar to that of UGS in the Urumqi River headwater area: it is also located on the southern slope of the mountain ridge and is small and thin, with an area of about 0.2 km<sup>2</sup> (Fig. 4k). The HDBC fresh moraine lies on top of older-looking

moraines (Fig. 4l) and is about 400 m away from the glacier front with a tarn formed in between. No previous numerical dating of glacial landforms has been conducted in the Haxilegen Pass area.

## 4. Methods

### 4.1. Geomorphic mapping and field sampling

Moraines that are fresh looking, sharp-crested, boulder-compact ridges located a few hundred meters down from a glacier terminus are usually assumed to have been formed during the LIA (Matthes, 1939; Shi and Ren, 1990; Owen, 2009). Previous studies have indicated that two or three lateral and/or terminal moraines were formed in the Central Asian highlands during different cold periods within the LIA (Shi and Ren, 1990; Su and Shi, 2002; Liu

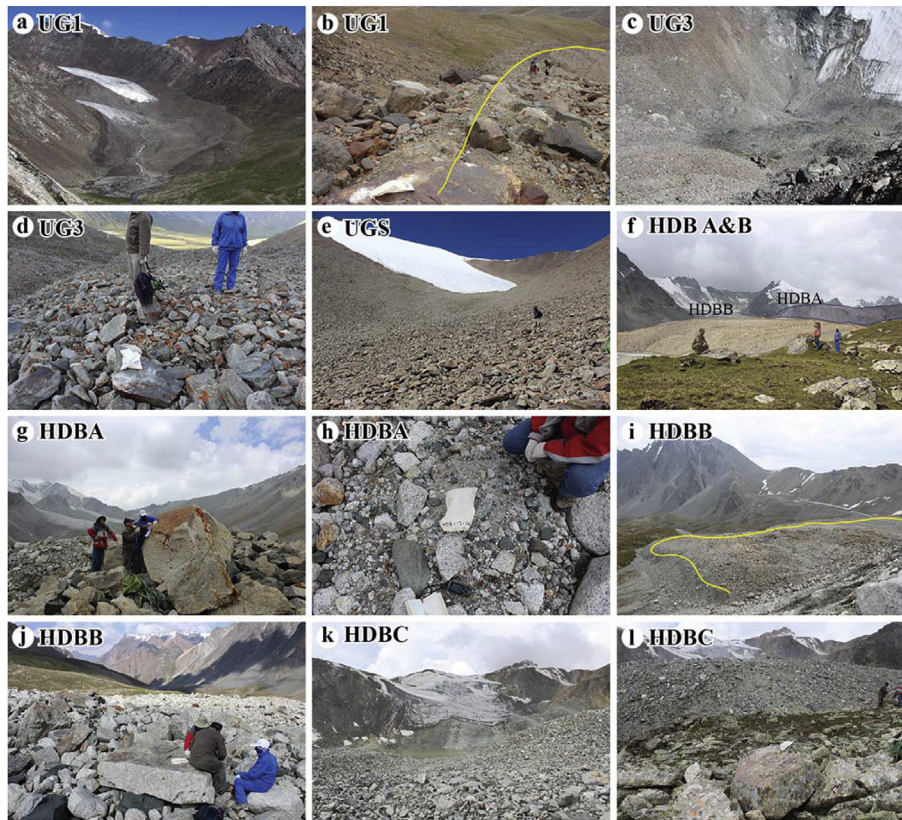


**Fig. 4.** Selected photos of field sites. a) An overview of the morphology of the LIA moraine at UG1. b) Lateral LIA moraine (yellow line) at UG1 and adjacent older moraine beyond the LIA moraine. c) Thin front of UG3 and its surrounding steep slopes. d) Standing on the rock debris of UG3 and looking east (downstream). The orange color is produced by lichen cover. e) Moraine materials in front of UGS on the southern side of the Daxi Valley. A man sitting on a rock for scale. f) A distant view of the moraines in front of HDBA and HDBB at Haxilegen Pass. The darker colored, higher HDBA moraine partially overlaps the lighter colored, lower HDBB moraine. They both override more vegetated, boulder-scattered, older glacial landforms. g) Sampling a large boulder at HDBA. h) Pebble sample of HDB-12-14 from HDBA. i) View of HDBB moraine extending to the highway. The yellow line indicates the fresh moraine boundary. j) Sampling a well-exposed large boulder at HDBB. k) The small HDBC glacier on the southern side of the Haxilegen Pass. A tarn is formed in front of the glacier terminus. l) Steep gradient seen from lower, older moraines at HDBC. (For interpretation of the references to colour in this figure legend, the reader is referred to the web version of this article.)

et al., 2003; Xu and Yi, 2014). The outermost moraine represents the maximum LIA glacial extent. Prior to the fieldwork, we identified and delineated these outermost moraines in Google Earth. We checked these moraines during the fieldwork in 2012 and also looked for twin or triplet moraine ridges that might be suitable for dating multiple LIA glacial advances.

We collected 1–4 cm thick rock chips (at least 1 kg) from the surfaces of quartz-rich boulders, using chisel and hammer, for  $^{10}\text{Be}$  exposure dating. Pebble samples were also collected at some sites to evaluate moraine surface stability by comparing the ages of boulders and pebbles (Briner, 2009; Heyman et al., 2011a). These samples were chosen from locations with minimal potential impact from shielding, movement, and overturning possibilities (Fig. 4). Detailed sample information was recorded in the field, and descriptions are provided in Table 1. The topographic shielding factor for each sample was calculated using a Python tool and a 90 m Shuttle Radar Topography Mission digital elevation model (DEM), with  $5^\circ$  as both azimuth interval and elevation angle interval (Li, 2013). Three to five samples at each presumed LIA moraine were collected to constrain the exposure age. At the headwater area of the Urumqi River, we collected three samples from the lateral moraine at the UG1 site to complement previous dating (Chen, 1989; Yi et al., 2004; Li et al., 2014), five samples from the UG3 fresh moraine, and three samples from the trace-lines in front of UGS. At the Haxilegen Pass, we collected ten samples at HDBA, including five samples from an inner moraine and five from an

outer moraine. We also collected five samples each from the fresh moraines at HDBB and HDBC, respectively. In total, 31 samples were collected from the presumed LIA moraines in these two areas to constrain the timing of the LIA glacial event using  $^{10}\text{Be}$  surface exposure dating.

#### 4.2. Laboratory methods

All samples were crushed and sieved to 250–500  $\mu\text{m}$  in the College of Urban and Environmental Sciences at Peking University. Physical and chemical preparations were conducted in the cosmogenic nuclide sample preparation laboratory at the University of Tennessee using standard procedures modified from Kohl and Nishiizumi (1992). After quartz separation and purification, about 1 g of each sample was extracted to check quartz purity using Olympus X-ray Fluorescence (XRF) and X-ray Diffraction (XRD) Analyzers. The purified quartz samples, ranging from 32.1 g to 102.3 g, were dissolved with an addition of 0.2–0.4 mg  $^9\text{Be}$  carrier using hydrofluoric acid. Then using chromatography columns and multiple precipitations, Be was extracted and purified to make a BeO target. The  $^{10}\text{Be}/^9\text{Be}$  ratios were measured using Accelerator Mass Spectrometry (AMS) at Purdue Rare Isotope Measurement Laboratory (PRIME Lab), Purdue University, based on the revised ICN standard (07KNSTD; Nishiizumi et al., 2007) and corrected with procedural blanks ( $2.5 \times 10^{-15}$ ). The  $^{10}\text{Be}/^9\text{Be}$  ratios were converted to  $^{10}\text{Be}$  concentrations for exposure age calculations (Table 1).

**Table 1**  
Sample information and  $^{10}\text{Be}$  concentration measurements used in this study.

Sample ID	Site	Latitude (°N)	Longitude (°E)	Elevation (m a.s.l.)	Rock type	Thickness (cm)	Topographic shielding factor	$^{10}\text{Be}$ concentration (atoms/g)
HDB-12-06	HDBA inner	43.7385	84.4024	3484	Quartzite	2	0.983	9435 ± 751
HDB-12-07	HDBA inner	43.7385	84.4025	3485	Quartzite	4	0.983	11,955 ± 1145
HDB-12-08	HDBA inner	43.7384	84.4028	3481	Granite	2.5	0.979	35,930 ± 3102
HDB-12-09	HDBA inner	43.7380	84.4033	3483	Granite	3	0.979	24,928 ± 1712
HDB-12-10	HDBA inner	43.7380	84.4034	3485	Granite	2	0.979	10,848 ± 1071
HDB-12-11	HDBA outer	43.7387	84.4032	3477	Granite	3	0.979	9502 ± 1616
HDB-12-12	HDBA outer	43.7385	84.4031	3475	Granite	2	0.979	18,203 ± 1757
HDB-12-13	HDBA outer	43.7387	84.4033	3473	Pebbles*	4	0.979	31,738 ± 1925
HDB-12-14	HDBA outer	43.7387	84.4032	3473	Pebbles	4	0.979	17,331 ± 1430
HDB-12-15	HDBA outer	43.7387	84.4032	3477	Quartzite	4	0.979	27,2712 ± 7051
HDB-12-16	HDBB	43.7372	84.4073	3411	Gneiss	3	0.971	11,313 ± 2434
HDB-12-17	HDBB	43.7373	84.4069	3418	Gneiss	2	0.973	5460 ± 859
HDB-12-18	HDBB	43.7372	84.4068	3417	Gneiss	4	0.973	10,562 ± 1602
HDB-12-19	HDBB	43.7372	84.4063	3420	Gneiss	4	0.973	13,193 ± 2339
HDB-12-20	HDBB	43.7370	84.4062	3424	Gneiss	4	0.973	9524 ± 1446
HDB-12-21	HDBC	43.7269	84.4120	3546	Granite	4	0.987	57,644 ± 3661
HDB-12-22	HDBC	43.7269	84.4121	3546	Granitic gneiss	3	0.987	447,984 ± 13,418
HDB-12-23	HDBC	43.7265	84.4124	3542	Granitic gneiss	3	0.986	347,687 ± 10,703
HDB-12-24	HDBC	43.7264	84.4127	3544	Granitic gneiss	4	0.987	202,972 ± 13,738
HDB-12-25	HDBC	43.7263	84.4128	3540	Granite	3	0.987	98,864 ± 2990
WY-12-02	Glacier No. 3 (UG3)	43.0995	86.8422	3635	Quartzite	3	0.917	446,260 ± 10,644
WY-12-03	Glacier No. 3 (UG3)	43.0996	86.8420	3638	Quartzite	4	0.917	30,961 ± 1264
WY-12-04	Glacier No. 3 (UG3)	43.0992	86.8418	3639	Quartzite	4	0.917	23,2496 ± 5855
WY-12-08	Glacier No. 3 (UG3)	43.0984	86.8412	3653	Quartzite	3	0.914	24,5356 ± 5922
WY-12-09	Glacier No. 3 (UG3)	43.0985	86.8412	3656	Quartz schist	2	0.914	13,1242 ± 6941
WY-12-15	Glacier at south (UGS)	43.0994	86.8067	3902	Granite	1	0.903	68,9854 ± 9066
WY-12-17	Glacier at south (UGS)	43.0991	86.8070	3888	Quartzite	2	0.903	15,99258 ± 20,073
WY-12-18	Glacier at south (UGS)	43.0992	86.8070	3877	Granite	4	0.903	1,098,607 ± 31,535
WY-12-21	Glacier No. 1 (UG1)	43.1176	86.8206	3785	Quartzite	1	0.970	13,915 ± 1693
WY-12-22	Glacier No. 1 (UG1)	43.1170	86.8216	3764	Quartzite	1	0.945	26,340 ± 7061
WY-12-23	Glacier No. 1 (UG1)	43.1167	86.8220	3758	Quartzite	2	0.945	10,027 ± 900

Note: \*: rock types for pebbles include mainly quartzite and granite pebbles; the topographic shielding was calculated using a Python tool (Li, 2013) with 5° intervals in both azimuth and altitude angles;  $^{10}\text{Be}$  concentration was converted from the AMS measured  $^{10}\text{Be}/^9\text{Be}$  ratios from PRIME lab at Purdue University.

Quartz weights,  $^9\text{Be}$  carrier masses, measured  $^{10}\text{Be}/^9\text{Be}$  ratios, and procedural blanks are listed in the [Supplementary table](#).

#### 4.3. Exposure age calculation and moraine age determination

Cosmogenic  $^{10}\text{Be}$  exposure ages were calculated using the CRONUS Earth 2.2 online calculator (Balco et al., 2008; <http://hess.ess.washington.edu/math/>) with an assumption of zero erosion (Lal, 1991). In the interpretation, we focus on ages derived from the Lal (1991)/Stone (2000) time-dependent scaling model (Table 2). We used the northeast North America production rate (NENA) (Balco et al., 2009), which is  $3.87 \pm 0.19$  atoms  $\text{g}^{-1} \text{yr}^{-1}$  for  $^{10}\text{Be}$ , as the reference production rate because most estimates of  $^{10}\text{Be}$  production rates published since Balco et al. (2009), with broad geographic coverage, generally agree within uncertainties with this value (e.g. Putnam et al., 2010; Heyman, 2014; Li et al., 2014; Lifton et al., 2014). Rock density was assigned as  $2.7 \text{ g cm}^{-3}$ . Other  $^{10}\text{Be}$  exposure ages during the LIA from previous publications (Li et al., 2014; Chen et al., 2015) were checked to ensure a consistent use of calculation scheme and data format with this study. Note that we reported both internal and external uncertainties for each  $^{10}\text{Be}$  exposure ages in Table 2. The internal uncertainty refers to only measurement uncertainty in the nuclide concentration; while the external uncertainty also includes uncertainties in the scaling model and the reference production rate (Balco et al., 2008). The

internal uncertainty is used in the inter-comparison of  $^{10}\text{Be}$  exposure ages from the eastern Tian Shan because the uncertainty in the nuclide production and scaling model are about the same for each sample in this relatively confined region (Balco et al., 2008). The external uncertainty is used to compare  $^{10}\text{Be}$  exposure ages with the ages from other dating techniques, such as radiocarbon and lichenometry. In the following discussion, we report the external uncertainty for a  $^{10}\text{Be}$  exposure age to be consistent with previous publications, but in the determination of age cluster (probability density and reduced chi-squared statistics as discussed below) for each moraine and comparing  $^{10}\text{Be}$  exposure ages among our study sites, we consider the internal uncertainty for an exposure age.

We plotted the probability density distribution of all  $^{10}\text{Be}$  exposure ages (with their internal uncertainties) for each moraine. These plots help identify age cluster(s) and potential outlier(s). Ideally, boulders on top of a moraine should produce exposure ages reflecting the moraine formation time, but exposure ages on a moraine are usually scattered due to complex geomorphic processes, which cannot be eliminated by averaging measurements of multiple samples (Balco et al., 2008; Heyman et al., 2011b). Different strategies have been used in interpreting scattered exposure ages and in identifying outliers. We used the reduced chi-squared test ( $\chi_R^2$ ) to test if the age scatter is due to measurement uncertainty (Balco and Schaefer, 2006; Balco, 2011; Li et al., 2014; Chen et al., 2015). If the  $\chi_R^2$  value is statistically significant

**Table 2**  
<sup>10</sup>Be surface exposure ages calculated using different scaling schemes.

Sample name	Moraine set, sample type	Constant Lal (1991)/Stone (2000)		Desilets and Zreda (2003); Desilets et al. (2006)		Dunai (2001)		Lifton et al. (2005)		Time-dependent Lal (1991)/Stone (2000)		Internal uncertainty (yr)
		Age (yr)	unc.*(yr)	Age (yr)	unc.(yr)	Age (yr)	unc.(yr)	Age (yr)	unc.(yr)	Age (yr)	unc.(yr)	
HDB-12-06	HDBA inner, boulder	201	19	204	19	194	18	202	19	222	21	16
HDB-12-07	HDBA inner, pebbles	259	28	263	28	250	27	260	28	286	31	25
HDB-12-08	HDBA inner, boulder	773	76	757	75	753	75	746	74	825	82	67
HDB-12-09	HDBA inner, boulder	538	45	542	46	520	44	536	45	587	49	37
HDB-12-10	HDBA inner, boulder	232	25	236	26	224	25	233	26	257	28	23
HDB-12-11	HDBA outer, boulder	206	36	209	37	199	35	207	37	228	40	35
HDB-12-12	HDBA outer, boulder	391	42	398	43	378	41	394	43	433	47	38
HDB-12-13	HDBA outer, pebbles	695	54	686	53	675	53	677	53	745	58	42
HDB-12-14	HDBA outer, pebbles	379	36	386	37	366	35	381	37	420	40	31
HDB-12-15	HDBA outer, boulder	5962	325	5461	302	5688	315	5360	296	5988	329	154
HDB-12-16	HDBB, boulder	256	57	262	58	249	55	259	57	284	63	55
HDB-12-17	HDBB, boulder	122	20	124	21	118	19	123	20	135	22	19
HDB-12-18	HDBB, boulder	240	38	245	39	233	37	242	39	266	42	36
HDB-12-19	HDBB, boulder	299	55	305	56	290	53	302	56	331	61	53
HDB-12-20	HDBB, boulder	216	34	220	35	209	33	218	35	238	38	33
HDB-12-21	HDDB, boulder	1201	96	1140	91	1171	94	1120	90	1251	100	76
HDB-12-22	HDDB, boulder	9276	526	8439	484	8720	501	8292	475	9263	528	278
HDB-12-23	HDDB, boulder	7219	412	6618	382	6934	401	6468	373	7204	414	223
HDB-12-24	HDDB, boulder	4237	352	3927	328	4158	347	3848	321	4310	359	287
HDB-12-25	HDDB, boulder	2050	116	1931	111	2097	121	1891	108	2126	121	62
WY-12-02	UG3, boulder	9606	516	8686	473	8988	490	8543	464	9595	519	230
WY-12-03	UG3, boulder	669	42	666	42	654	42	659	42	722	46	27
WY-12-04	UG3, boulder	5029	273	4652	256	4923	271	4571	251	5088	278	127
WY-12-08	UG3, boulder	5240	282	4830	263	5092	278	4745	258	5291	286	127
WY-12-09	UG3, boulder	2773	198	2626	189	2858	206	2583	186	2882	207	147
WY-12-15	UGS, boulder	12,831	640	11,174	566	11,406	579	11,029	558	12,779	643	169
WY-12-17	UGS, boulder	30,354	1517	24,879	1261	24,786	1258	24,437	1236	29,050	1462	384
WY-12-18	UGS, boulder	21,279	1196	17,917	1019	17,978	1023	17,666	1003	20,784	1175	614
WY-12-21	UG1, boulder	256	33	260	34	246	32	258	34	284	37	31
WY-12-22	UG1, boulder	503	137	510	139	485	132	506	138	553	151	135
WY-12-23	UG1, boulder	194	20	197	20	187	19	195	20	215	22	17

Note: \*: unc. stands for the external uncertainty. We used the CRONUS-Earth 2.2 online calculator (Balco et al., 2008) to calculate all exposure ages. In the calculation, we assumed zero surface erosion, and used the Northeast North America (NENA) <sup>10</sup>Be production rate as the reference production rate (Balco et al., 2009). The ages derived from the time-dependent Lal (1991)/Stone (2000) scaling scheme are used in the study. We used the ages listed in this table to determine reduced  $\chi^2$  statistics and the weighted mean ages (with uncertainty); but in the text and figures, we rounded the ages to 10s (reported as yr) for the ages of <1.0 kyr and 100s for the ages of >1.0 kyr (reported as kyr).

( $p < 0.05$ ), the variation in ages cannot be explained solely by measurement errors and the age scatter is likely caused by geomorphic processes. In this case, we removed the ages outside the cluster to refine the  $\chi^2_R$  value and re-test its significance. If ages are excessively scattered and do not overlap within the error, no age can be used to represent the age for the moraine. If the  $\chi^2_R$  value is not statistically significant ( $p > 0.05$ ), the variation in ages can be explained by measurement errors alone (Chen et al., 2015) and, in this case, the weighted mean of the ages is assigned as the age of the moraine.

## 5. Results

### 5.1. Urumqi River headwaters

Three samples (WY-12-21, 22, 23) from the UG1 lateral moraine produced exposure ages of  $220 \pm 20$  yr,  $280 \pm 40$  yr, and  $550 \pm 150$  yr. Four previously published <sup>10</sup>Be ages from the terminal moraine at this site have clustered ages with a weighted mean of  $400 \pm 70$  yr (Li et al., 2014). The whole group of <sup>10</sup>Be ages ranges from  $220 \pm 20$  yr to  $550 \pm 150$  yr, within the span of the LIA period (Table 2; Fig. 5a). The reduced chi-squared statistic on this group of seven samples is 18.2 ( $p < 0.05$ ), indicating that the scatter of these ages is not solely caused by measurement uncertainty. Two of the three samples from the lateral moraine are much younger than other ages. These boulders might have experienced some incomplete exposure, such as toppling or shielding from other boulders,

causing apparently younger surface exposure ages. Another possibility is that these two young boulders around 250 yr were actually produced by a later glacial advance. After removing these two young ages,  $\chi^2_R$  is reduced to 1.3 ( $p > 0.05$ ), allowing for the use of the weighted mean of the five remaining ages ( $430 \pm 110$  yr) to represent the moraine age. We therefore assigned the weighted mean age of  $430 \pm 110$  yr for the outermost LIA moraine in front of UG1 (Fig. 5a). This age is consistent with the ages constrained by lichenometry (1595–1650 CE; Chen, 1989) and similar to two <sup>14</sup>C ages ( $1550 \text{ CE} \pm 120$  and  $1520 \pm 120$ ) originally reported in Yi et al. (2004) and recalculated by Xu and Yi (2014). Such consistent ages derived from multiple methods confirm the timing of the maximum LIA glacial advance at UG1.

The adjacent site, UG3, however, yielded five exposure ages ranging from  $720 \pm 50$  yr to  $9.6 \pm 0.5$  kyr (Table 2). A large  $\chi^2_R$  of 5551.3 suggests that geomorphic processes played a critical role in the scatter of the ages (Fig. 5b). These ages are much older than the LIA and widely scattered, so we do not assign an age to this moraine. Similarly at UGS site, three exposure ages are all >10 kyr without overlap, yielding a large  $\chi^2_R$  of 1373.2 (Table 2; Fig. 5c). Due to the widely scattered ages, we also hesitate to assign an age to the trace-line of UGS.

### 5.2. Haxilegen Pass

Five samples (HDB-12-06 to 10) from the HDBA inner fresh moraine produced exposure ages ranging from  $220 \pm 20$  yr to

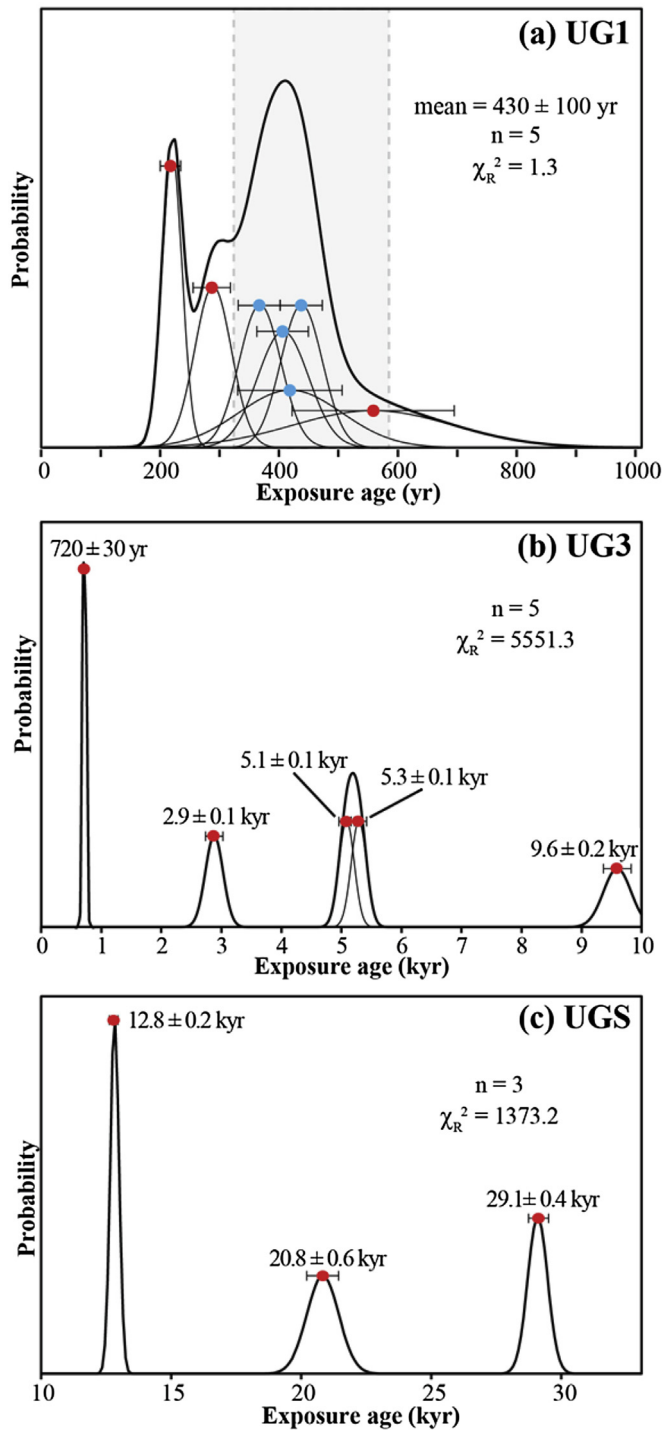


**Fig. 5.** Probability density plot of  $^{10}\text{Be}$  surface exposure ages for fresh moraine sets at UG1, UG3, and UGS sites. (a) Five samples highlighted at UG1 produced a small value of reduced chi-square statistic ( $\chi^2_R$ ), and the weighted mean ( $430 \pm 110$  yr) was calculated. Blue points represent ages from Li et al. (2014); (b) Five samples at UG3 produced a large value of  $\chi^2_R$ , and no age was assigned to this landform; (c) Three samples at UGS also produced a large  $\chi^2_R$ , and no age was assigned to this landform as well. (Note: internal uncertainty was used for data shown in this figure.)

$830 \pm 80$  yr (Table 2). The probability density plot shows that three young ages are clustered, and two older ages,  $590 \pm 50$  yr and  $830 \pm 80$  yr, do not overlap with this cluster (Fig. 6a). These two older ages may reflect boulders incorporated from an earlier LIA glacial advance, or they might have fallen from valley sidewall on

the glacier with prior exposure and then were mixed with HDBA's younger boulders. Removing these two older ages reduces the  $\chi^2_R$  value from 81.1 ( $p < 0.05$ ) to 2.9 ( $p > 0.05$ ). We used the weighted mean of the three young exposure ages,  $260 \pm 40$  yr, as the age for the HDBA inner moraine. The pebble sample at this site, HDB-12-07, yielded an exposure age of  $290 \pm 30$  yr, consistent with the two young boulder samples. The similarity between pebble and boulder exposure ages indicates that pebbles and boulders might have experienced similar exposure histories (Briner, 2009; Heyman et al., 2011a).

The exposure ages of five samples (HDB-12-10 to 15) from the HDBA outer moraine show an interesting pattern: four samples have ages within 1.0 kyr, but one sample, HDB-12-15, produced an age of  $6.0 \pm 0.3$  kyr, likely representing an outlier (Table 2; Fig. 6b). After removing this outlier, the other four exposure ages are still scattered ( $\chi^2_R = 30.5$ ,  $p < 0.05$ ). The youngest boulder ( $230 \pm 40$  yr) might have experienced incomplete exposure due to post-depositional processes, such as toppling and exhumation, or might indicate the presence of a young glacial event. The older age ( $750 \pm 60$  yr) might be from the boulder incorporated from an early LIA glacial advance or from the boulder fallen from the valley sides/headwalls with prior exposure. The remaining two samples are clustered at  $430 \pm 40$  yr ( $\chi^2_R = 0.07$ ,  $p > 0.05$ ). Considering the possibility that different LIA glacial advances might reach a similar extent and incorporate boulders from previous events or boulders fallen from the valley sides/headwalls, we tentatively assigned the weighted mean of these two clustered ages,  $430 \pm 40$  yr, as the formation age of the HDBA outer moraine.

Five boulder samples (HDB-12-16 to 20) taken from the HDBB fresh moraine produced exposure ages ranging from  $140 \pm 20$  yr to  $330 \pm 60$  yr (Table 2). The probability density plot shows that the youngest age is likely not part of the cluster of the other four ages (Fig. 6c). This youngest boulder might have experienced incomplete exposure. After removing this youngest age, the remaining four ages are highly clustered between  $240 \pm 40$  yr and  $330 \pm 60$  yr, with a  $\chi^2_R$  value of 0.9 ( $p > 0.05$ ). The weighted mean of these four ages,  $280 \pm 60$  yr, was assigned as the age of the HDBB moraine, similar to the age of the HDBA inner moraine.

The five exposure ages from HDBC at the southern side of the Haxilegen Pass show an extremely scattered pattern ( $\chi^2_R = 1123.2$ ,  $p < 0.05$ ), ranging from  $1.3 \pm 0.1$  kyr to  $9.3 \pm 0.5$  kyr (Fig. 6d). The widely scattered ages are likely caused by geomorphic processes and prevent us to assign a formation age for this moraine.

## 6. Discussion

### 6.1. Cosmogenic $^{10}\text{Be}$ surface exposure dating of LIA moraines

Four moraine groups (UG1, HDBA inner, HDBA outer, and HDBB in Figs. 5a and 6a–c, respectively) produce robust age clusters that can be used to constrain the formation of the moraines during the LIA, although a few apparently old or young outliers were excluded in the age determination. Apparently old outliers are likely the result of nuclide inheritance that may be introduced by incorporating boulders from prior glacial events, or boulders that were exposed on valley sides or headwalls and then incorporated into the moraine by falling, sliding, creeping, or other supraglacial processes. Apparently young outliers are possibly from the boulders that experienced incomplete exposure due to post-glacial exhumation or toppling, or the mixing of boulders from a later event due to the close proximity of the inner and the outer moraines (Figs. 2b and 3b).

In contrast,  $^{10}\text{Be}$  ages from fresh-looking moraines in front of UG3, HDBC, and UGS are up to tens of thousands of years older than the LIA and are widely scattered. Would these widely scattered and

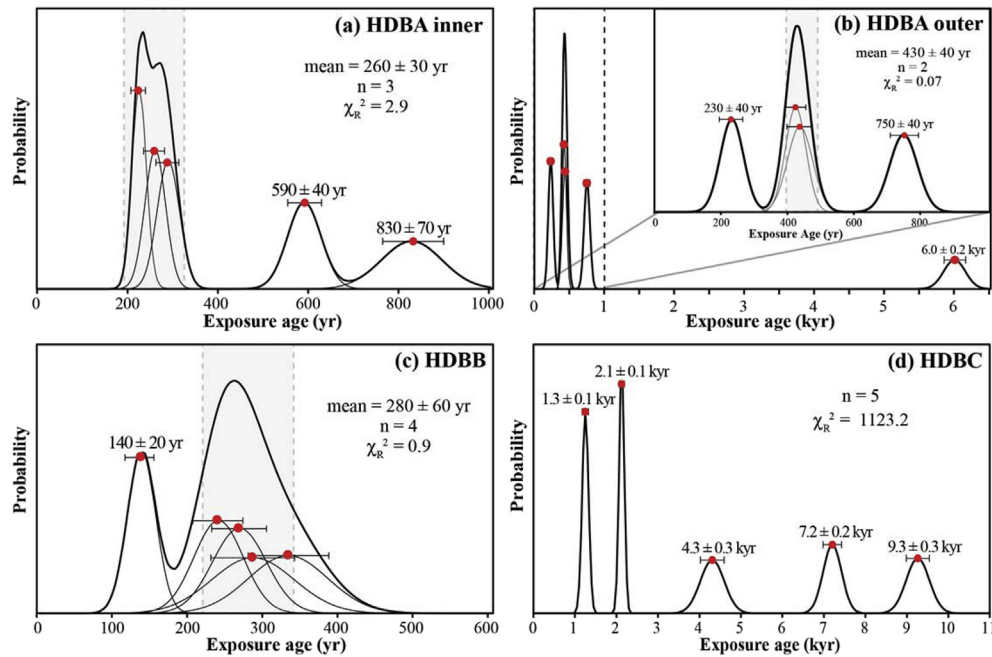


**Fig. 6.** Probability density plot of  $^{10}\text{Be}$  surface exposure ages for fresh moraine sets at the Haxilegen Pass sites. Each site has five samples. In (a), (b), and (c), the assigned ages of the moraines are highlighted using dashed grey bars, with calculated weighted mean and  $\chi_R^2$ . (d) Five samples at HDBC produced widely scattered ages, and no age was assigned to this landform. (Note: internal uncertainty was used for data shown in this figure).

much older ages indicate that these moraines were formed much earlier than the LIA, suggesting that these glaciers did not have any clear advances during the LIA? To examine the past fluctuations of these glaciers, we checked 1:50,000 topographic maps produced in China based on aerial photos in the early 1960s. The topographic maps indicate that UG3 and HDBC were much more extensive than their current positions and some of our sample locations were in fact covered by ice in the early 1960s (Figs. 2a and 3a), while UGS terminus has maintained a similar position comparing the 1960s extent to present extent (Fig. 2a). It seems that these glaciers have behaved similarly with those glaciers with constrained LIA ages, such as UG1, HDBA, and HDBB. Therefore, the moraines we sampled in front of these three glaciers likely also mark the extent of glaciers during the LIA, but the apparent exposure ages from our sampled boulders do not reflect the actual moraine formation age. We interpret that the much older and widely scattered exposure ages from these moraines are caused by considerable and varied nuclide inheritance. One potential source of nuclide inheritance comes from the boulders that were exposed on valley sides or headwalls and later incorporated into the moraine by falling, sliding, creeping, or other supraglacial processes. As discussed earlier, we also observed some outliers on well-constrained LIA moraines from UG1, HDBA, and HDBB that may be related to this type of nuclide inheritance, but the fraction of this type of inheritance is small and does not affect the determination of the moraine ages (the majority of the ages from other samples are within the range of the LIA). In contrast, almost all exposure ages we obtained from the moraines in front of UG3, UGS, and HDBC are much older than the LIA and widely scattered. Thus, the pattern of much old and widely scattered exposure ages in front of these glaciers is likely caused by other geomorphic processes. Note that all these three glaciers are small and thin glaciers. Glacial erosion under these glaciers in the continental climate of Central Asia has likely been limited and not powerful enough to produce fresh boulders with zero initial nuclide concentration. Instead, these glaciers might have only

disturbed and reworked materials that were originally deposited prior to the LIA by early glacial advances or other geomorphic processes, such as fluvial and slope processes. Varied nuclide concentrations of such reworked materials might be removed during glacial transport in the LIA. Therefore, samples collected from such moraines may produce widely scattered and much older ages due to considerable and varied nuclide inheritance.

## 6.2. Timing of LIA glacial advances in the Tian Shan

Four of the moraines we sampled have ages consistent with the LIA (Figs. 5a and 6a–c). The UG1 and HDBA outermost moraines were dated to similar ages and indicate a maximum LIA glacial advance at  $430 \pm 100$  yr, a weighted mean of  $430 \pm 110$  yr at UG1 and  $430 \pm 40$  yr at outer HDBA. The HDBA inner moraine and HDBB yielded close ages around  $270 \pm 55$  yr, a weighted mean of  $260 \pm 40$  yr at inner HDBA and  $280 \pm 60$  yr at HDBB, indicating a possible late glacial advance during the LIA. Although these two weighted mean ages are almost overlapped, they more likely represent two separated events if only considering internal uncertainties (90 yr and 50 yr, respectively) in the comparison. At HDBA site, these two events are constrained from the outer and inner moraines, and at HDBB site, the sampled moraine ( $280 \pm 60$  yr) is correlated to the late event. Such indication of two LIA glacial advances is consistent with previous descriptions of LIA moraines in western China that include two or three sub-moraines (Shi and Ren, 1990; Su and Shi, 2002; Liu et al., 2003; Xu and Yi, 2014). More high-precision dating work is needed to constrain the timing of separated LIA events more accurately.

In the easternmost Tian Shan, Chen et al. (2015) reported 11  $^{10}\text{Be}$  exposure ages from fresh-looking moraines (M1) in front of the glacier at the Turgan Valley in the Karlik Range (Fig. 1). After removing five old ages ( $\chi_R^2$  value reduced from 84.1 to 1.4), their data assemble a moraine age of  $790 \pm 300$  yr (recalculated; internal uncertainty: 280 yr), representing an earlier LIA advance. However,

in Chen et al. (2015), M1 is still not the outermost ridge of the fresh-looking moraine set, indicating that an even older glacial event than  $790 \pm 300$  yr might exist in the easternmost Tian Shan.

In summary, cosmogenic  $^{10}\text{Be}$  exposure ages obtained from our study areas, along with other available  $^{10}\text{Be}$  ages from the easternmost Tian Shan, suggest that glaciers advanced at least three times during the LIA: the first advance occurred at  $790 \pm 300$  yr; the second advance around  $430 \pm 100$  yr; and the last one at  $270 \pm 55$  yr.

### 6.3. The extent of LIA glacial advances in the Tian Shan

The extent of LIA glacial advances can be measured using a variety of parameters, and we used the distance from the LIA moraines to the front of present-day glaciers and the equilibrium line altitude (ELA) change from LIA glacier to present-day glaciers to quantify glacier changes during the investigated period. The distances were directly measured from Google Earth; and the ELA were estimated using the toe-to-summit altitude method (TSAM), which calculates the mean elevation between the highest peak within the glacier catchment and the terminus of each glacier at a certain period (Benn and Lehmkuhl, 2000). This method has been broadly applied to glaciers on the Tibetan Plateau and Mongolia (Benn and Lehmkuhl, 2000). We used the absolute value to represent the ELA changes ( $\Delta\text{ELA}$ ) from the LIA to the present.

For the Urumqi River headwaters, the outermost LIA moraine is located about 700 m beyond the lower branch of the UG1 glacier snout, and the ELA depression during the LIA glacial advance was about 50 m (based on the terminal elevation of the lower branch) (Table 3). For the Haxilegen Pass, the  $^{10}\text{Be}$  dated LIA moraines (including the inner and outer moraine ridges located close to each other) are within 900 m beyond the glacier snout, and the ELA depressions for HDBA and HDBB during the LIA were estimated to be 40 m and 60 m, respectively (Table 3). In the easternmost Tian Shan, the fresh moraines dated to the LIA by Chen et al. (2015) are up to 800 m away from the present glacier terminus, and the ELA depression was calculated as 60 m in their study. Both the distances (700–900 m) retreated since the LIA maximum glacial extent and the ELA depressions (40–60 m) during the LIA show less extensive LIA glacial advances in the eastern Tian Shan than that in the western Tian Shan (Kyrgyz Tian Shan). Specifically, Solomina et al. (2004) examined retreats of 293 glaciers since the LIA in the Kyrgyz Tian Shan using 1980s aerial photographs and lichenometric dating and found a retreat distance of  $989 \pm 540$  m on average. Considering that there has been continuous glacial retreat after the 1980s in the Kyrgyz Tian Shan, the distance from the outermost LIA moraines to the front of present-day glaciers could be over 1 km. They also estimated ELA depressions to be about 75–100 m, using the same TSAM (Solomina et al., 2004). Using the accumulation-area ratio (AAR) method, Porter (1970) provided an estimate of the  $\Delta\text{ELA}$  range of 100–150 m during the LIA for the temperate zone of the Northern Hemisphere. Such comparisons suggest that the LIA glacial event in the eastern Tian Shan is likely less extensive than the western Tian Shan and other temperate zones of the

Northern Hemisphere.

Although  $^{10}\text{Be}$  ages did not produce a conclusive age for the moraines/trace-lines at UG3, UGS, and HDBC, the glacial extent on the 1960s topographic maps (Figs. 2a and 3a) suggests that 1) UG3 and HDBC might have retained much of their LIA extent through to the 1960s, or they might have retreated at the end of the LIA and then re-advanced to this extent by the 1960s; and 2) all glaciers have shrunk significantly within the most recent 50 years, which is consistent with remote sensing based studies in the Tian Shan (e.g. Ding et al., 2006; Bolch, 2007; Li et al., 2008). If the maximum LIA extents at UG3 and HDBC were the same as the presumed LIA extent, these small and thin glaciers had expanded their ice coverage about 400 m in distance and about 20–25 m in ELA depression compared to their present terminus positions. The relatively large ELA depression of UGS (Table 3) is probably caused by local steep topography. Variations in retreat distance and  $\Delta\text{ELA}$  from different glaciers indicate that glacier change are not only affected by climate change, but also affected by local topographic and geometric factors, such as glacier size, elevation, slope, and aspect (Li and Li, 2014).

### 6.4. Climate imprint on LIA glacial advances

Climate conditions in Central Asia during the last millennium have been reconstructed from a range of proxy data (Figs. 1 and 7). High-frequency climate records from tree rings, ice cores, and other proxies indicate that the coldest period in Central Asia occurred during the 17th century (~400 yr), which was also a period of high precipitation (Fig. 7; Yang et al., 2009). Ice core oxygen isotope record from the Dunde Ice Cap in the Qilian Shan revealed that several cold periods occurred around 600 yr, 400 yr and 200 yr, among which the coldest period is 400 yr (Fig. 7; Yao et al., 1997; Thompson et al., 2006). To the south of our study sites, aeolian sediment analysis in the Tarim Basin indicates wet conditions during the period of 100–500 yr, and two distinct clay layers formed in a wet, depositional environment at ~380–450 yr (Fig. 7; Liu et al., 2011). Such a cold and wet climate around 400 yr in Central Asia could explain the maximum LIA glacial advance around  $430 \pm 100$  yr in our study area.

The glacial advance of  $270 \pm 55$  yr also corresponds to a cold-wet period indicated in proxy records. For example, the carbonate content in a sediment core from Bosten Lake (Fig. 1) reflects the strongest cold and humid conditions around 250 yr (Fig. 7; Chen et al., 2006). An early LIA glacial advance at  $790 \pm 300$  yr does not coincide with distinct cold or wet periods in the proxy records, but does coincide with a slight temperature depression in the Northern Hemisphere and the development of permafrost in the western Tian Shan (Fig. 7; Marchenko and Gorbunov, 1997; Esper et al., 2003; Moberg et al., 2005). Admittedly, the fluctuations in some climate proxy data may not correspond well to three LIA glacial events constrained from LIA moraines in the Tian Shan, and even opposite trends can be observed, such as relatively high  $\delta^{18}\text{O}$  in Dunde ice core and high temperature in tree ring records of Central Asia and Kyrgyz Tian Shan during the earliest LIA event around 800 yr. Note that paleoclimatic proxy data are rare at high elevations close to our sample sites, and more climate proxy related studies from surrounding environment are needed to reconstruct the past climate in this area.

It seems that the maximum LIA glacial advance occurred asynchronously across the eastern Tian Shan. Although the maximum LIA extent of relatively large and thick glaciers is similar at the Urumqi River headwater and the Haxilegen Pass of our study area and the Karlik Range in the easternmost Tian Shan, the timing of this extent is much earlier ( $790 \pm 300$  yr) at the Karlik Range than the timing of our two study sites ( $430 \pm 100$  yr). Such variations

**Table 3**

Glacier area, retreat distance, and estimated change in ELA ( $\Delta\text{ELA}$ ) from LIA glaciers to present-day glaciers at our sites and the Karlik Range.

	UG1	UG3	UGS	HDBA	HDBB	HDBC	Karlik
Area (km <sup>2</sup> )	1.6	0.4	0.2	1.1	1.2	0.2	6.8
Distance (m)	700	400	400	900	900	400	800
$\Delta\text{ELA}$ (m)	50	20	55	40	60	25	60

Note:  $\Delta\text{ELA}$  for the Karlik Range is modified from Chen et al. (2015), in which the TSAM was also applied.

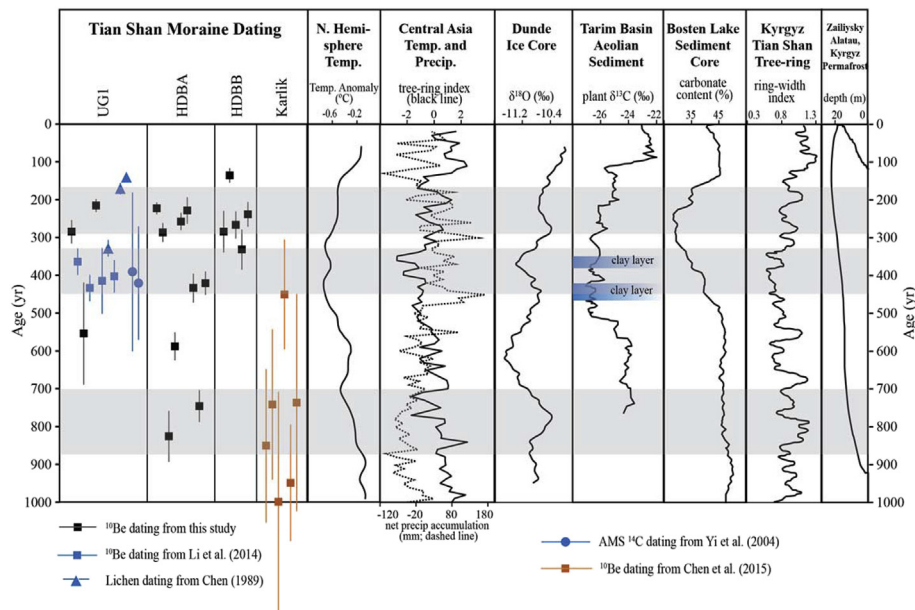


**Fig. 7.** Comparison of dated moraine records in the Tian Shan and selected published climate records: N. Hemisphere temperature (Moberg et al., 2005); Central Asia temperature and precipitation (Yang et al., 2009); Dunde ice core (Thompson et al., 2006); Tarim Basin aeolian sediment (Liu et al., 2011); Bosten Lake sediment core (Chen et al., 2006); Kyrgyz Tian Shan tree rings (Esper et al., 2003); and Zailiysky, Alatau, Kyrgyz permafrost (Marchenko and Gorbunov, 1997).

were potentially affected by regional climate pattern and orographic effects. Large water bodies, such as the Caspian Sea, the Aral Sea, and Lake Issyk-Kul, serve as major sources of atmospheric moisture transported by the westerlies to the Tian Shan (Kreutz et al., 1997; Benn and Owen, 1998; Aizen et al., 2001). Glaciers are developed at high elevations in response to temporal shifts of the westerlies, which interact with the mountain topography to form a west-east decreasing gradient of precipitation in the Tian Shan (Sorg et al., 2012). Several studies (e.g. Karpychev, 2005; Sorrel et al., 2006; Boomer et al., 2009) have reconstructed high lake levels close to the moisture source area around 400 yr, consistent with the cold and wet period suggested by climate proxy data in Central Asia. This period is also the time when the maximum glacial advance occurred in the Urumqi River headwaters and at the Haxilegen Pass, but restricted advances might occur during this period in the easternmost Tian Shan. One possible explanation could be that decreased precipitation from west to east due to the orographic effect might cause less ice/snow accumulation in the easternmost range than to the west. The difference in the timing and extent of LIA glacial advances between our sites and other regions of the Tian Shan suggests that more work are necessary to better understand the spatial pattern of the climate systems and their temporal variations across the Tian Shan.

## 7. Conclusions

We used  $^{10}\text{Be}$  surface exposure dating of 31 samples collected from fresh moraines at the Urumqi River headwater and the Haxilegen Pass to constrain the timing and pattern of LIA glacial advances in the eastern Tian Shan, China. The outermost moraines in front of glaciers larger than  $1.0\text{ km}^2$  produced well-clustered ages around  $430 \pm 100\text{ yr}$ , indicating that the moraines were formed during the LIA. This glacial advance was a response to the cold and humid climate around 400 yr, as reconstructed from other proxy data in Central Asia. We also constrained a slightly less extensive glacial advance that occurred around  $270 \pm 55\text{ yr}$ , corresponding to another cold and humid period in the 18th century.

Samples from fresh moraines in front of small and thin glaciers

produced widely scattered and much older ages than the LIA. These samples may have originated from events prior to the LIA advances with considerable and varied nuclide inheritance. Small and thin glaciers are not erosive and may not produce enough fresh boulders with initial zero nuclide concentration; instead, they might primarily rework previously-deposited materials that were already exposed prior to the LIA glacial advances, producing apparently much older and widely scattered exposure ages.

Cosmogenic  $^{10}\text{Be}$  ages for LIA glacial advances across the eastern Tian Shan indicate that the maximum LIA extent ( $\sim 800\text{ m}$  in retreat distance and  $\sim 50\text{ m}$  in ELA changes) occurred during  $790 \pm 300\text{ yr}$  in the easternmost range, but  $430 \pm 100\text{ yr}$  at our study sites. It is possible that an early LIA glacial advance occurred at our sites but was overridden by a later and more extensive LIA advance. The more restricted advance of glaciers in the easternmost range in  $430 \pm 100\text{ yr}$  likely reflects reduced moisture availability from the westerlies. Additional chronological and proxy data are needed to better understand the spatio-temporal pattern of LIA glacial advances and its driving factors.

## Acknowledgments

This work was funded by the National Natural Science Foundation of China (41328001, 41230523, and 40971002), the National Geographic Society Young Explorers Grant (9086-12), and the National Science Foundation Doctoral Dissertation Improvement Research Grant (BCS-1303175). We would like to thank Rebecca Potter and Dakota Anderson for assisting the lab work, and Xiulin Shen and Junxi Kang for assisting in the fieldwork. We appreciate Guocheng Dong, Mei Zhang, and the College of Urban and Environmental Sciences at Peking University, China, for initial sample processing and shipping. We are grateful to Susan Ma, Tom Clifton, and Greg Chmiel at the PRIME Lab for providing lab training and sample measurements. We thank Carol Harden and Henri Grissino-Mayer for providing improvements in writing. We thank Jakob Heyman and an anonymous reviewer for their constructive comments and suggestions.

## Appendix A. Supplementary data

Supplementary data related to this article can be found at <http://dx.doi.org/10.1016/j.quascirev.2016.02.023>.

## References

- Aizen, E.M., Aizen, V.B., Melack, J.M., Nakamura, T., Ohta, T., 2001. Precipitation and atmospheric circulation patterns at mid-latitudes of Asia. *Int. J. Climatol.* 21, 535–556.
- Aizen, V.B., Aizen, E.M., Joswiak, D.R., Fujita, K., Takeuchi, N., Nikitin, S.A., 2006. Climatic and atmospheric circulation pattern variability from ice-core isotope/geochemistry records (Altai, Tien Shan and Tibet). *Ann. Glaciol.* 43, 49–60.
- Aizen, V.B., Aizen, E.M., Melack, J.M., Dozier, J., 1997. Climatic and hydrologic changes in the Tien Shan, Central Asia. *J. Climatol.* 10, 1393–1404.
- Balco, G., 2011. Contributions and unrealized potential contributions of cosmogenic-nuclide exposure dating to glacier chronology, 1990–2010. *Quat. Sci. Rev.* 30, 3–27.
- Balco, G., Briner, J., Finkel, R.C., Rayburn, J.A., Ridge, J.C., Schaefer, J.M., 2009. Regional beryllium-10 production rate calibration for late-glacial northeastern North America. *Quat. Geochronol.* 4, 93–107.
- Balco, G., Schaefer, J.M., 2006. Cosmogenic-nuclide and varve chronologies for the deglaciation of southern New England. *Quat. Geochronol.* 1, 15–28.
- Balco, G., Stone, J.O., Lifton, N.A., Dunai, T.J., 2008. A complete and easily accessible means of calculating surface exposure ages or erosion rates from  $^{10}\text{Be}$  and  $^{26}\text{Al}$  measurements. *Quat. Geochronol.* 3, 174–195.
- Barclay, D.J., Wiles, G.C., Calkin, P.E., 2009. Holocene glacier fluctuations in Alaska. *Quat. Sci. Rev.* 28, 2034–2048.
- Benedict, J.B., 1968. Recent glacial history of an alpine area in the Colorado Front Range, USA. II: dating the glacial deposits. *J. Glaciol.* 7, 77–87.
- Benn, D.I., Lehmkühl, F., 2000. Mass balance and equilibrium-line altitudes of glaciers in high mountain environments. *Quatern. Int.* 65/66, 15–29.
- Benn, D.I., Owen, L.A., 1998. The role of the Indian summer monsoon and the mid-latitude westerlies in Himalayan glaciation: review and speculative discussion. *J. Geol. Soc.* 155, 353–363.
- Bolch, T., 2007. Climate change and glacier retreat in northern Tien Shan (Kazakhstan/Kyrgyzstan) using remote sensing data. *Glob. Planet. Change* 56, 1–12.
- Boomer, I., Wunnemann, B., Mackay, A.W., Austin, P., Sorrel, P., Reinhardt, C., Keyser, D., Guichard, F., Fontugne, M., 2009. Advances in understanding the late Holocene history of the Aral Sea region. *Quat. Int.* 194, 79–90.
- Bradley, R.S., Jones, P.D., 1993. 'Little Ice Age' summer temperature variations: their nature and relevance to recent global warming trends. *Holocene* 3, 367–376.
- Bräuning, A., 2006. Tree-ring evidence of 'Little Ice Age' glacier advances in southern Tibet. *Holocene* 16, 369–380.
- Briner, J.P., 2009. Moraine pebbles and boulders yield indistinguishable  $^{10}\text{Be}$  ages: a case study from Colorado, USA. *Quat. Geochronol.* 4, 299–305.
- Chen, F., Yuan, Y.J., Chen, F.H., Wei, W.S., Yu, S.L., Chen, X.J., Fan, Z.A., Zhang, R.B., Zhang, T.W., Shang, H.M., Qin, L., 2013. A 426-year drought history for Western Tien Shan, Central Asia, inferred from tree rings and linkages to the North Atlantic and Indo–West Pacific Oceans. *Holocene* 23, 1095–1104.
- Chen, F.H., Huang, X.Z., Zhang, J.W., Holmes, J.A., Chen, J.H., 2006. Humid Little Ice Age in and Central Asia documented by Bosten Lake, Xinjiang, China. *Sci. China Ser. D Earth Sci.* 49, 1280–1290.
- Chen, F.H., Yu, Z.C., Yang, M.L., Ito, E., Wang, S.M., Madsen, D.B., Huang, X.Z., Zhao, Y., Sato, T., Birks, H.J.B., Boomer, I., Chen, J.H., An, C.B., Wunnemann, B., 2008. Holocene moisture evolution in arid central Asia and its out-of-phase relationship with Asian monsoon history. *Quat. Sci. Rev.* 27, 351–364.
- Chen, J., 1989. Preliminary researches on lichenometric chronology of Holocene glacial fluctuations and on other topics in the headwater of Urumqi River, Tianshan Mountains. *Sci. China Ser. B Chem.* 32, 1487–1500.
- Chen, Y., Li, Y., Wang, Y., Zhang, M., Cui, Z., Yi, C., Liu, G., 2015. Late Quaternary glacial history of the Karlik Range, easternmost Tian Shan, derived from  $^{10}\text{Be}$  surface exposure and optically stimulated luminescence datings. *Quat. Sci. Rev.* 115, 17–27.
- Chenet, M., Roussel, E., Jomelli, V., Grancher, D., 2010. Asynchronous Little Ice Age glacial maximum extent in southeast Iceland. *Geomorphology* 114, 253–260.
- Cui, Z., 1981. Glacial erosion landforms and development of trough at the head of Urumqi River, Tian Shan. *J. Glaciol. Geocryol.* 3, 1–15 (in Chinese).
- Derbyshire, E., Li, J., Perrott, F., Xu, S., Waters, R., 1984. Quaternary Glacial History of the Hunza Valley, Karakoram Mountains, Pakistan. *The International Karakoram Project* 2, pp. 456–495.
- Desilets, D., Zreda, M., 2003. Spatial and temporal distribution of secondary cosmic-ray neutron intensities and applications to in situ cosmogenic dating. *Earth Planet. Sci. Lett.* 206, 21–42.
- Desilets, D., Zreda, M., Prabu, T., 2006. Extended scaling factors for in situ cosmogenic nuclides: new measurements at low latitude. *Earth Planet. Sci. Lett.* 246, 265–276.
- Ding, Y., Liu, S., Li, J., Shangguan, D., 2006. The retreat of glaciers in response to recent climate warming in western China. *Ann. Glaciol.* 43, 97–105.
- Dunai, T., 2001. Influence of secular variation of the geomagnetic field on production rates of in situ produced cosmogenic nuclides. *Earth Planet. Sci. Lett.* 193, 197–212.
- Esper, J., Shiyatov, S.G., Mazepa, V.S., Wilson, R.J.S., Graybill, D.A., Funkhouser, G., 2003. Temperature-sensitive Tien Shan tree ring chronologies show multi-centennial growth trends. *Clim. Dynam.* 21, 699–706.
- Finkel, R.C., Owen, L.A., Barnard, P.L., Caffee, M.W., 2003. Beryllium-10 dating of Mount Everest moraines indicates a strong monsoon influence and glacial synchronicity throughout the Himalaya. *Geology* 31, 561–564.
- Gong, D.Y., Ho, C.H., 2002. The Siberian High and climate change over middle to high latitude Asia. *Theor. Appl. Climatol.* 72, 1–9.
- Gosse, J.C., Phillips, F.M., 2001. Terrestrial in situ cosmogenic nuclides: theory and application. *Quat. Sci. Rev.* 20, 1475–1560.
- Grove, J.M., 2004. In: *Little Ice Ages: Ancient and Modern*, vol. 2. Routledge, London.
- Harrison, S., Winchester, V., Glasser, N.F., 2007. The timing and nature of recession of outlet glaciers of Hielo Patagonico Norte, Chile, from their Neoglacial IV (Little Ice Age) maximum positions. *Glob. Planet. Change* 59, 67–78.
- Heyman, J., Stroeven, A.P., Caffee, M.W., Hattestrand, C., Harbor, J.M., Li, Y., Alexanderson, H., Zhou, L., Hubbard, A., 2011a. Palaeoglaciology of Bayan Har Shan, NE Tibetan Plateau: exposure ages reveal a missing LGM expansion. *Quat. Sci. Rev.* 30, 1988–2001.
- Heyman, J., Stroeven, A.P., Harbor, J.M., Caffee, M.W., 2011b. Too young or too old: evaluating cosmogenic exposure dating based on an analysis of compiled boulder exposure ages. *Earth Planet. Sci. Lett.* 302, 71–80.
- Heyman, J., 2014. Paleoglaciation of the Tibetan Plateau and surrounding mountains based on exposure ages and ELA depression estimates. *Quat. Sci. Rev.* 91, 30–41.
- Ivy-Ochs, S., Kober, F., 2008. Surface exposure dating with cosmogenic nuclides. *Eiszeitalt. Ggw.* 57, 179–209.
- Jiao, K.Q., Iwata, S., Yao, T.D., Jing, Z.F., Li, Z.Q., 2005. Variation of Zepu Glacier and environmental change in the eastern Nyainqentanglha range since 3.2 ka BP. *J. Glaciol. Geocryol.* 27, 74–79.
- Kaban, M., Yuanda, T., 2014. Density structure, isostatic balance and Tectonic models of the Central Tien Shan. *Surv. Geophys.* 35, 1375–1391.
- Karpychev, Y.A., 2005. Transgressive-regressive stages of the Caspian Sea for the last 20 ky inferred from radiocarbon dating of the coastal and bottom sediments. *Oceanology* 45, 420–430.
- Kelly, M.A., Lowell, T.V., Hall, B.L., Schaefer, J.M., Finkel, R.C., Goehring, B.M., Alley, R.B., Denton, G.H., 2008. A 10Be chronology of lateglacial and Holocene mountain glaciation in the Scoresby Sund region, east Greenland: implications for seasonality during lateglacial time. *Quat. Sci. Rev.* 27, 2273–2282.
- Koch, J., Kilian, R., 2005. 'Little Ice Age' glacier fluctuations, Gran Campo Nevado, southernmost Chile. *Holocene* 15, 20–28.
- Kohl, C.P., Nishiizumi, K., 1992. Chemical isolation of quartz for measurement of in situ-produced cosmogenic nuclides. *Geochim. Cosmochim. Acta* 56, 3583–3587.
- Kong, P., Fink, D., Na, C., Huang, F., 2009. Late Quaternary glaciation of the Tianshan, Central Asia, using cosmogenic  $^{10}\text{Be}$  surface exposure dating. *Quat. Res.* 72, 229–233.
- Koppes, M., Gillespie, A.R., Burke, R.M., Thompson, S.C., Stone, J., 2008. Late quaternary glaciation in the Kyrgyz Tien Shan. *Quat. Sci. Rev.* 27, 846–866.
- Kreutz, K., Mayewski, P., Meeker, L., Twickler, M., Whitlow, S., Pittalwala, I., 1997. Bipolar changes in atmospheric circulation during the Little Ice Age. *Science* 277, 1294–1296.
- Lal, D., 1991. Cosmic ray labeling of erosion surfaces: in situ nuclide production rates and erosion models. *Earth Planet. Sci. Lett.* 104, 424–439.
- Li, Y.K., Liu, G.N., Cui, Z.J., 2001a. Glacial valley cross-profile morphology, Tian Shan Mountains, China. *Geomorphology* 38, 153–166.
- Li, Y.K., Liu, G.N., Cui, Z.J., 2001b. Longitudinal variations in cross-section morphology along a glacial valley: a case-study from the Tien Shan, China. *J. Glaciol.* 47, 243–250.
- Li, Y.K., 2013. Determining topographic shielding from digital elevation models for cosmogenic nuclide analysis: a GIS approach and field validation. *J. Mt. Sci.* 10, 355–362.
- Li, Y.K., Harbor, J., 2009. Cosmogenic nuclides and geomorphology: Theory, limitations, and applications. In: Ferrari, D.M., Guiseppe, A.R. (Eds.), *Geomorphology and Plate Tectonics*. Nova Science Publishers, Inc, Hauppauge, New York, pp. 1–33.
- Li, Y.K., Liu, G.N., Chen, Y.X., Li, Y.N., Harbor, J., Stroeven, A.P., Caffee, M., Zhang, M., Li, C.C., Cui, Z.J., 2014. Timing and extent of quaternary glaciations in the Tianger Range, eastern Tian Shan, China, investigated using  $^{10}\text{Be}$  surface exposure dating. *Quat. Sci. Rev.* 98, 7–23.
- Li, Y.K., Liu, G.N., Kong, P., Harbor, J., Chen, Y.X., Caffee, M., 2011. Cosmogenic nuclide constraints on glacial chronology in the source area of the Urumqi River, Tian Shan, China. *J. Quat. Sci.* 26, 297–304.
- Li, Y.N., Li, Y.K., 2014. Topographic and geometric controls on glacier changes in the central Tien Shan, China, since the Little Ice Age. *Ann. Glaciol.* 55, 177–186.
- Li, Z.Q., Shen, Y.P., Li, H.L., Dong, Z.W., Wang, L.W., 2008. Response of the melting Urumqi glacier No. 1 in Eastern Tianshan to climate change. *Adv. Clim. Change Res. (Suppl. 4)*, 67–72.
- Lifton, N., Beel, C., Hattestrand, C., Kassab, C., Rogozhina, I., Heermance, R., Oskin, M., Burbank, D., Blomdin, R., Gribenski, N., Caffee, M., Goehring, B.M., Heyman, J., Ivanov, M., Li, Y., Li, Y., Petrakov, D., Usabaliev, R., Codilean, A.T., Chen, Y., 2014. Constraints on the late Quaternary glacial history of the Inylchek and Sary-Dzaz valleys from in situ cosmogenic  $^{10}\text{Be}$  and  $^{26}\text{Al}$ , eastern Kyrgyz Tian Shan. *Quat. Sci. Rev.* 101, 77–90.
- Lifton, N.A., Bieber, J.W., Clem, J.M., Duldig, M.L., Evenson, P., Humble, J.E., Pyle, R., 2005. Addressing solar modulation and long-term uncertainties in scaling secondary cosmic rays for in situ cosmogenic nuclide applications. *Earth Planet.*

- Sci. Lett. 239, 140–161.
- Liu, G.N., Xiong, H.G., 1992. The denudation rate of gelifraction and its influential factors in the periglacial environment of Tianshan Mountains (in China). *J. Glaciol. Geocryol.* 14, 333–341.
- Liu, G.N., Xiong, H.G., Cui, Z.J., Song, C.Q., 1995. The morphological features and environmental condition of rockglaciers in Tianshan Mt. *Sci. Geogr. Sin.* 15, 226–233 (in Chinese with English abstract).
- Liu, S.Y., Sun, W.X., Shen, Y.P., Li, G., 2003. Glacier changes since the Little Ice Age maximum in the western Qilian Shan, northwest China, and consequences of glacier runoff for water supply. *J. Glaciol.* 49, 117–124.
- Liu, W.G., Liu, Z.H., An, Z.S., Wang, X.L., Chang, H., 2011. Wet climate during the 'Little Ice Age' in the arid Tarim Basin, northwestern China. *Holocene* 21, 409–416.
- Loso, M.G., Doak, D.F., Anderson, R.S., 2014. Lichenometric dating of Little Ice Age glacier moraines using explicit demographic models of lichen colonization, growth, and survival. *Geogr. Ann. A Phys. Geogr.* 96, 21–41.
- Luckman, B.H., 2000. The Little Ice Age in the Canadian Rockies. *Geomorphology* 32, 357–384.
- Luthi, M.P., 2014. Little Ice Age climate reconstruction from ensemble reanalysis of Alpine glacier fluctuations. *Cryosphere* 8, 639–650.
- Mann, M.E., 2002. Little ice age. *Encycl. Glob. Environ. Change* 1, 504–509.
- Mann, M.E., Bradley, R.S., Hughes, M.K., 1999. Northern hemisphere temperatures during the past millennium: inferences, uncertainties, and limitations. *Geophys. Res. Lett.* 26, 759–762.
- Mann, M.E., Zhang, Z., Hughes, M.K., Bradley, R.S., Miller, S.K., Rutherford, S., Ni, F., 2008. Proxy-based reconstructions of hemispheric and global surface temperature variations over the past two millennia. *P. Natl. Acad. Sci. U. S. A.* 105, 13252–13257.
- Mann, M.E., Zhang, Z.H., Rutherford, S., Bradley, R.S., Hughes, M.K., Shindell, D., Ammann, C., Faluvegi, G., Ni, F.B., 2009. Global signatures and dynamical origins of the Little Ice Age and medieval climate anomaly. *Science* 326, 1256–1260.
- Marchenko, S.S., Gorbunov, A.P., 1997. Permafrost changes in the northern Tien Shan during the Holocene. *Permafrost. Periglac.* 8, 427–435.
- Matthes, F.E., 1939. Report of Committee on Glaciers, April 1939. *Eos. Transactions American Geophysical Union* 20, pp. 518–523.
- Moberg, A., Sonechkin, D.M., Holmgren, K., Datsenko, N.M., Karlen, W., 2005. Highly variable Northern Hemisphere temperatures reconstructed from low- and high-resolution proxy data. *Nature* 433, 613–617.
- Mosley-Thompson, E., Thompson, L.G., Grootes, P.M., Gundestrup, N., 1990. Little ice age (neoglaciation) paleoenvironmental conditions at siple station, Antarctica. *Ann. Glaciol.* 14, 199–204.
- Narama, C., Kondo, R., Tsukamoto, S., Kajiura, T., Ormukov, C., Abdrakhmatov, K., 2007. OSL dating of glacial deposits during the last glacial in the Terskey-Alatau Range, Kyrgyz Republic. *Quat. Geochronol.* 2, 249–254.
- Nishiizumi, K., Imamura, M., Caffee, M., Southon, J., Finkel, R., McAnich, J., 2007. Absolute calibration of <sup>10</sup>Be AMS standards. *Nucl. Instrum. Meth. B* 258, 403–413.
- Owen, L.A., 2009. Latest Pleistocene and Holocene glacier fluctuations in the Himalaya and Tibet. *Quat. Sci. Rev.* 28, 2150–2164.
- Owen, L.A., Finkel, R.C., Barnard, P.L., Ma, H.Z., Asahi, K., Caffee, M.W., Derbyshire, E., 2005. Climatic and topographic controls on the style and timing of Late Quaternary glaciation throughout Tibet and the Himalaya defined by Be-10 cosmogenic radionuclide surface exposure dating. *Quat. Sci. Rev.* 24, 1391–1411.
- Porter, S.C., 1970. Quaternary glacial record in Swat Kohistan, west Pakistan. *Geol. Soc. Am. Bull.* 81, 1421–1446.
- Putnam, A.E., Schaefer, J.M., Barrell, D.J.A., Vandergoes, M., Denton, G.H., Kaplan, M.R., Finkel, R.C., Schwartz, R., Goehring, B.M., Kelley, S.E., 2010. In situ cosmogenic Be-10 production-rate calibration from the Southern Alps, New Zealand. *Quat. Geochronol.* 5, 392–409.
- Schaefer, J.M., Denton, G.H., Kaplan, M.R., Putnam, A., Finkel, R.C., Barrell, D.J.A., Andersen, B.G., Schwartz, R., Mackintosh, A., Chinn, T., Schluchter, C., 2009. High-frequency Holocene glacier fluctuations in New Zealand differ from the northern signature. *Science* 324, 622–625.
- Seong, Y.B., Owen, L.A., Yi, C.L., Finkel, R.C., Schoenbohm, L., 2009. Geomorphology of anomalously high glaciated mountains at the northwestern end of Tibet: Muztag Ata and Kongur Shan. *Geomorphology* 103, 227–250.
- Shi, Y., Ren, J., 1990. Glacier recession and lake shrinkage indicating a climatic warming and drying trend in central Asia. *Ann. Glaciol.* 14, 261–265.
- Solomina, O., Barry, R., Bodnya, M., 2004. The retreat of Tien Shan glaciers (Kyrgyzstan) since the Little Ice Age estimated from aerial photographs, lichenometric and historical data. *Geogr. Ann. A Phys. Geogr.* 86, 205–215.
- Sorg, A., Bolch, T., Stoffel, M., Solomina, O., Beniston, M., 2012. Climate change impacts on glaciers and runoff in Tien Shan (Central Asia). *Nat. Clim. Chang.* 2, 725–731.
- Sorrel, P., Popescu, S.M., Head, M.J., Suc, J.P., Klotz, S., Oberhansli, H., 2006. Hydrographic development of the Aral Sea during the last 2000 years based on a quantitative analysis of dinoflagellate cysts. *Paleogeogr. Paleoclimatol. Paleocool.* 234, 304–327.
- Stone, J.O., 2000. Air pressure and cosmogenic isotope production. *J. Geophys. Res. Sol. EA* 105, 23753–23759.
- Su, Z., Shi, Y., 2002. Response of monsoonal temperate glaciers to global warming since the Little Ice Age. *Quat. Int.* 97–98, 123–131.
- Thompson, L.G., Mosley-Thompson, E., Brecher, H., Davis, M., Leo, B., Les, D., Lin, P.N., Mashiotta, T., Mountain, K., 2006. Abrupt tropical climate change: past and present. *P. Natl. Acad. Sci.* 103, 10536–10543.
- Wang, J., 1981. Ancient glaciers at the head of Urumqi river, Tian Shan. *J. Glaciol. Geocryol.* 3, 55–63 (in Chinese).
- Wang, Z., 1993. Surface runoff variations since Little Ice Age in the Daxigou-Urumqi River. *Adv. Water Sci.* 4, 260–267 (in Chinese with English abstract).
- Winsor, K., Carlson, A., Rood, D., 2014. <sup>10</sup>Be dating of the Narsarsuaq moraine in southernmost Greenland: evidence for a late-Holocene ice advance exceeding the Little Ice Age maximum. *Quat. Sci. Rev.* 98, 135–143.
- Xu, X., Yi, C., 2014. Little Ice Age on the Tibetan Plateau and its bordering mountains: evidence from moraine chronologies. *Glob. Planet. Change* 116, 41–53.
- Yang, H., Qiu, S., 1965. Quaternary glaciation and the post-glacial climatic fluctuations in the region of upper Urumqi valley. *Sink. Sci. Geogr. Sin.* 31, 194–211 (in Chinese).
- Yang, B., Wang, J.S., Bräuning, A., Dong, Z.B., Esper, J., 2009. Late Holocene climatic and environmental changes in and central Asia. *Quat. Int.* 194, 68–78.
- Yao, T., Shi, Y., Thompson, L.G., 1997. High resolution record of paleoclimate since the Little Ice Age from the Tibetan ice cores. *Quat. Int.* 37, 19–23.
- Ye, B., Yang, D., Jiao, K., Han, T., Jin, Z., Yang, H., Li, Z., 2005. The Urumqi River source Glacier No. 1, Tianshan, China: changes over the past 45 years. *Geophys. Res. Lett.* 32, L21504.
- Yi, C., Jiao, K., Liu, K., He, Y., Ye, Y., 2002. ESR dating of the sediments of the last glaciation at the source area of the Urumqi River, Tian Shan Mountains, China. *Quat. Int.* 97–8, 141–146.
- Yi, C., Liu, K., Cui, Z., Jiao, K., Yao, T., He, Y., 2004. AMS radiocarbon dating of late quaternary glacial landforms, source of the Urumqi River, Tien Shan—a pilot study of <sup>14</sup>C dating on inorganic carbon. *Quat. Int.* 121, 99–107.
- Yin, A., Harrison, T.M., 2000. Geologic evolution of the Himalayan-Tibetan orogen. *Ann. Rev. Earth Pl. Sci.* 28, 211–280.
- Zech, R., 2012. A late Pleistocene glacial chronology from the Kitschi-Kurumdu Valley, Tien Shan (Kyrgyzstan), based on Be-10 surface exposure dating. *Quat. Res.* 77, 281–288.
- Zhao, J., Zhou, S., He, Y., Ye, Y., Liu, S., 2006. ESR dating of glacial tills and glaciations in the Urumqi River headwaters, Tianshan Mountains, China. *Quat. Int.* 144, 61–67.
- Zheng, B., 1990. The glacier, environment and its changes since the last glaciation in West China. *Quatern. Sci.* 2, 101–110.
- Zheng, B., Zhang, Z., 1983. Fluctuation of glaciers during Neoglaciation in Bogda and the Urumqi River head, Tianshan. *J. Glaciol. Geocryol.* 5, 133–142 (in Chinese).